Journal of Medicinal Chemistry

pubs.acs.org/jmc

Article

Grapefruit Extracellular-Vesicle-Derived Nanodrug Loading Three-Functional Platinum(IV) Conjugates with Enhanced Targeting and TME Modulating Properties

Yan Chen, Shuaiqi Feng, Lanjie Li, Guiqin Liu, Qingshan Ma, Zhifang Liu, Yanna Zhao, and Qingpeng Wang*

Cite This: J. Med. Chem. 2025, 68, 11928−11947

Read Online

ACCESS | Metrics & More | Article Recommendations | Supporting Information

ABSTRACT: Grapefruit extracellular vesicle (GEVs) derived nanodrug Tf-GEVs@Pt(IV) loading novel three-functional platinum(IV) conjugates was developed, which was effective in modulating the inflammatory, fibrotic, and immunosuppressive tumor microenvironment (TME). The GEVs enhanced the penetration of Tf-GEVs@Pt(IV) into tumor tissues, while the transferrin (Tf) moiety further improved the tumor-targeting capabilities. The active ingredient, platinum(IV) conjugate, was released in a sustained manner within the TME, which was easily reduced to platinum(II), aspirin (ASP), and captopril (CTP) fragments. The platinum core caused significant DNA damage. The inflammatory TME was ameliorated by inhibiting COX-2 and reducing TNF-α and IL-6 through the synergistic actions of GEVs and ASP. Collagen fibrosis was disrupted by the CTP moiety, which downregulated TGF-β1, MMP2, and MMP9. Consequently, the immunologically 'cold' TME was transformed into a 'hot' state by inhibiting PD-L1 and activating cGAS/STING pathways. Then, the T-cell activation and macrophage polarization from the M2- to M1-phenotype were provoked in tumor tissues.

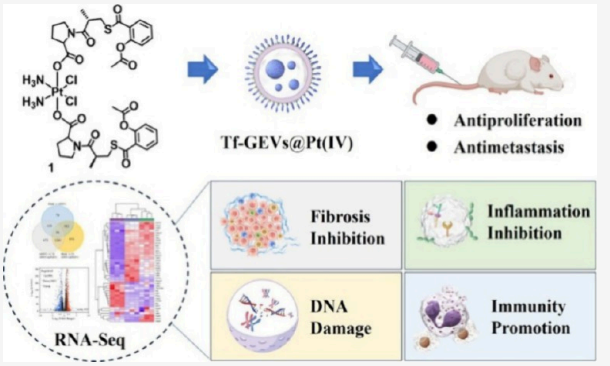

INTRODUCTION

Cancers are still major threats to human health, despite the rapid development of multiple cancer treatment methods.[1,2] In particular, metastatic tumors are the leading cause of death, accounting for over 90% of mortality among cancer patients. Chemotherapy remains a primary cancer treatment. However, the complex tumor microenvironment (TME) erects a robust protective barrier for tumors, which significantly contributes to the failure of chemotherapy.[3,4] Remodeling the TME during cancer treatment holds great promise for enhancing the effectiveness of antitumor drugs and offers a new horizon in the fight against cancer.

Tumor fibrosis, characterized by deposition, remodeling, and cross-linking of the extracellular matrix (ECM), has increasingly been recognized as an important component of the TME, which is now appreciated as a key factor in fostering malignant transformation and tumor aggression.[5−9] Tumor-associated inflammation (TAI), as a characteristic of the TME, has great potential to increase the levels of collagen biosynthesis by promoting factors such as TGF-β and MMPs, thereby accelerating the fibrosis process in tumors.[10−13] More importantly, the fibrotic and inflammatory TME display synergetic roles in recruiting the "cold" immunosuppressive TME. The dense collagen fibrosis physically prevented immune cells and drugs from efficiently infiltrating into the tumor. Meanwhile, the TAI was also effective in initiating the immune checkpoint PD-L1/PD-1 cascades by secreting COX-2 and cytokines such as TNF-α and IL-6, which further triggered macrophage polarization toward the pro-tumorigenic M2 subtype and promoted T-cell exhaustion.[14−17] Accordingly, targeting the fibrotic and inflammatory TME and further converting the 'cold' immune environment to a 'hot' status appears to be a promising approach to inhibit tumor growth and metastasis.

Platinum drugs are the most representative metal-based chemotherapeutic agents, accounting for almost 50% of regimens in clinical settings.[18,19] Nevertheless, inherent drawbacks, such as easily acquired drug resistance, serious toxicity, and poor tumor targeting properties, significantly hinder their clinical outcomes. There is a growing body of evidence supporting the significant involvement of the formation of TME in causing the failure of platinum-based

Received: March 22, 2025
Revised: April 28, 2025
Accepted: May 14, 2025
Published: May 26, 2025

https://doi.org/10.1021/acs.jmedchem.5c00815
J. Med. Chem. 2025, 68, 11928−11947

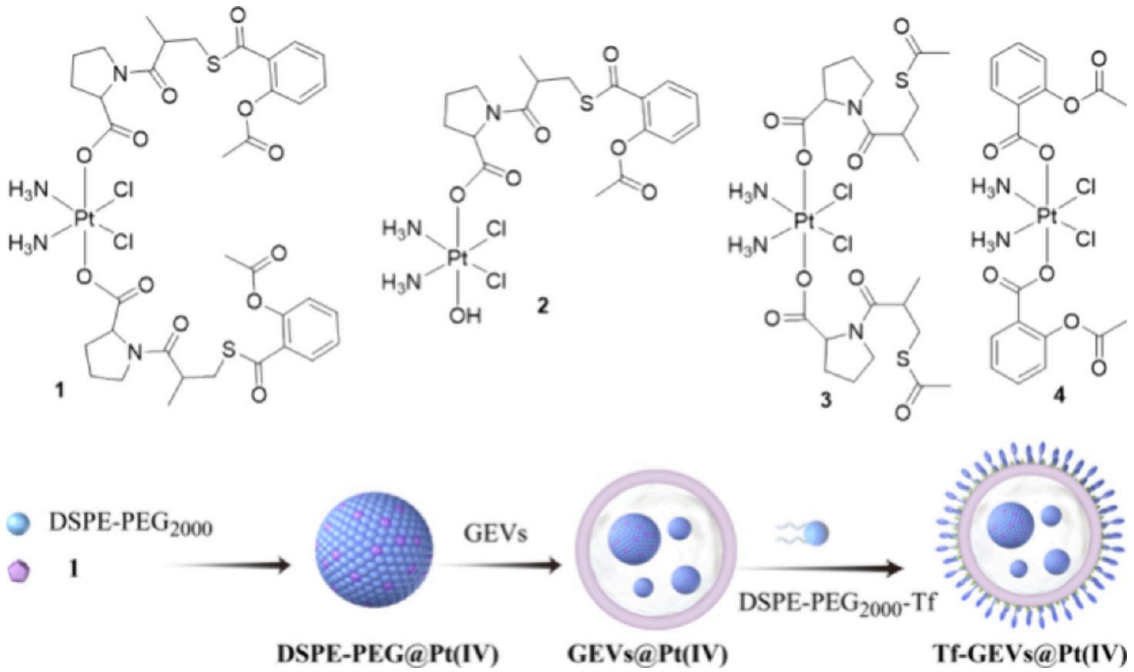

Figure 1. Structures of platinum(IV) complexes **1**−**4**, and nanodrugs GEVs@Pt(IV) and Tf-GEVs@Pt(IV).

chemotherapy.[20,21] Platinum(IV) conjugates as prodrugs of platinum(II) drugs offer a meaningful way to overcome these drawbacks by incorporating diverse functional ligands in the axial positions.[22,23]

Aspirin (ASP), a nonsteroidal anti-inflammatory drug, has been extensively proven to have great potential in suppressing TAI. Dual-functional platinum(IV) complexes bearing ASP ligands have been investigated as antitumor agents, exhibiting antiproliferative and antimetastatic properties by targeting COXs and MMPs, in addition to causing DNA damage.[24,25] Moreover, captopril (CTP) as an effective angiotensin converting enzyme (ACE) inhibitor was proven effective in suppressing the fibrosis through downregulating key enzymes MMPs and TGF-β1.[26−28] Considering these observations, we rationally developed three-functional platinum(IV) conjugates **1**−**2** by incorporating a new ligand CTP-ASP (Figure 1). These conjugates were expected to display potent antitumor activities by inhibiting the fibrotic and inflammatory TME, damaging DNA, and further reversing the immune-suppressive TME.

Tumor-targeted therapy has emerged as a remarkable advancement in cancer treatment and has become a hot topic in the development of new antitumor drugs. Delivering platinum complexes using nanodrug delivery systems (NDDS) is a promising strategy to enhance their tumor-targeting properties.[29,30] The development of extracellular vesicles (EVs) as NDDS, especially plant-derived EVs (PDVs), has attracted rapidly growing attention over the past decade for their superiorities as follows[31−34]: (1) Structurally, PDVs are lipid-bound structures capable of encapsulating both hydrophilic and hydrophobic cargos within the aqueous core or the lipid bilayer. (2) PDVs are promising in decreasing the risk of immunogenicity and toxicity in comparison with conventional synthetic carriers, as well as mammalian-derived EVs. (3) PDVs are effective in preventing the hydrolysis of drugs and provide tailorable drug release. (4) The extensive sources of plants provide cost-effective, sustainable, and renewable "nanofactories" for producing PDVs. (5) More importantly, PDVs have great potential for crossing the collagen fibrous barrier to deliver drugs into tumor tissues. Recently, some agents based on PDVs have been developed and progressed to clinical trials, which have opened a new frontier for modern drug delivery. However, the potential of PDVs in delivering platinum(IV) drugs has not yet been studied, which warrants extensive investigation to further determine their impact on antitumor performance.

The grapefruit-derived extracellular vesicles (GEVs), as typical PDVs, display fascinating performance against tumor cells with no detectable toxicity, meanwhile, they are also effective in reducing inflammation by decreasing the expression of pro-inflammatory cytokines and chemokines.[35] Moreover, the investigation of GEVs as drug carriers has attracted increasing attention, demonstrating great potential in reducing the side effects of the encapsulated drugs and improving their therapeutic efficacy, all while inducing no immunogenic response.[36] Whereas the lack of tumor-specific targeting profiles is still a key factor restricting their development, the surface membrane engineering modification of GEVs with tumor-targeting motifs appears to be a direct and promising strategy to enhance their tumor targeting properties.[37] As is widely known, the transferrin receptor (TfR) is overexpressed on the surface of diverse tumor cells due to the strong demand for iron during the unrestricted proliferation of tumors. Thereby, transferrin (Tf) is frequently selected for the modification of nanodrugs because of its promising tumor-targeting capabilities.[38−40] Notably, the potency of Tf in enhancing the tumor-targeting effects of PDVs has not yet been studied. Herein, a Tf-decorated GEVs system was developed for the first time with the expectation of improving tumor-targeting competence.

Inspired by the observations above and as a continuation of our interest in developing novel antitumor agents, three-functionalized platinum(IV) conjugates **1**−**2** with dual or mono CTP-ASP ligands were designed and prepared. As

https://doi.org/10.1021/acs.jmedchem.5c00815
J. Med. Chem. 2025, 68, 11928−11947

Scheme 1. Synthetic Procedure of Platinum(IV) Complexes 1−4

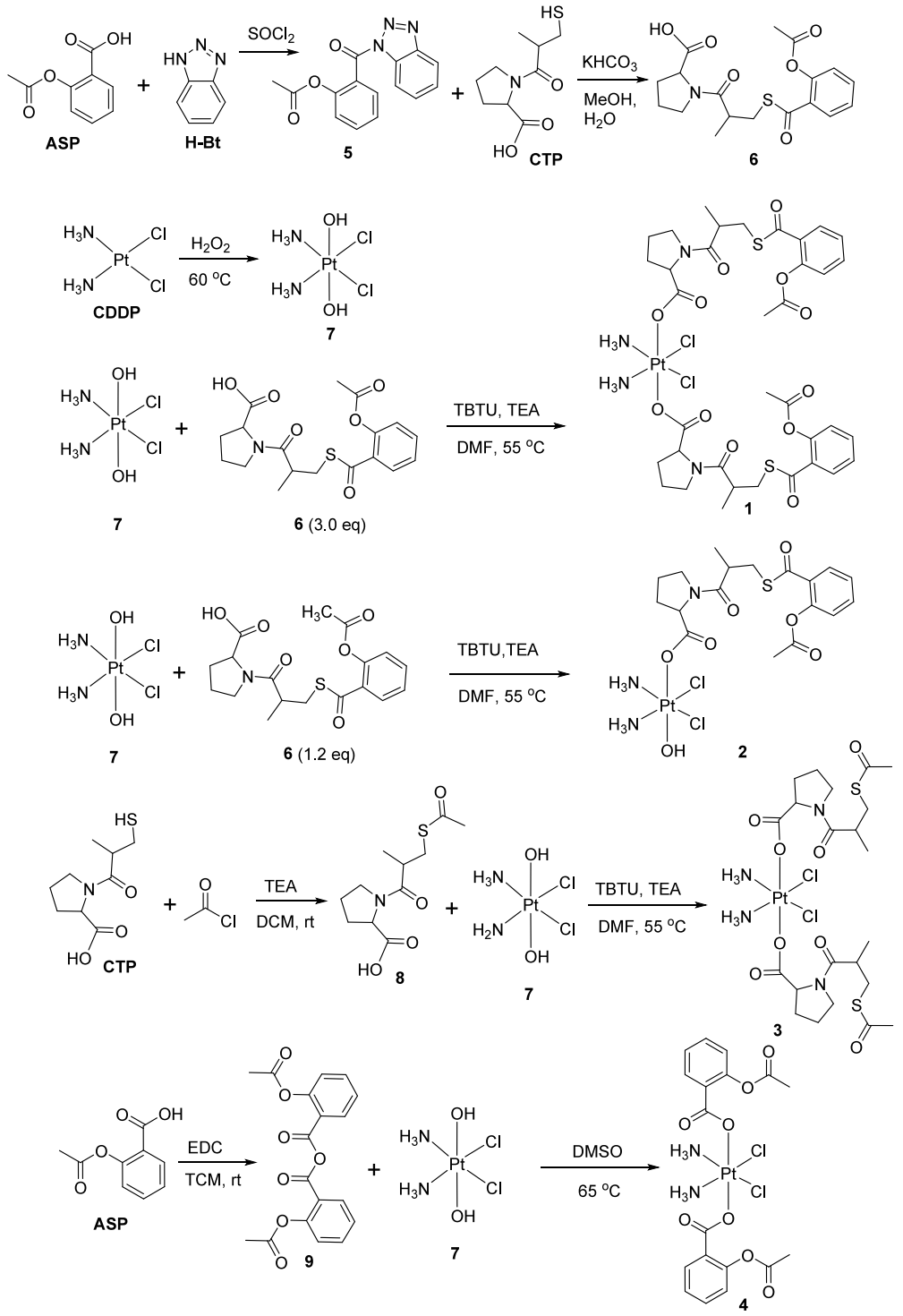

reference drugs, dual-functional platinum(IV) complex **3** with CTP ligands and complex **4** with ASP ligands were also prepared. After primary antitumor evaluation in vitro, conjugate **1** with dual CTP-ASP ligands was screened out as the candidate. Subsequently, nanodrug GEVs@Pt(IV) encapsulating conjugate **1** was prepared. Then, Tf was incorporated to yield nanoparticles Tf-GEVs@Pt(IV), aiming to further improve the tumor targeting properties. The antiproliferative, antimetastatic, tumor-targeting, and immunity-modulating properties were evaluated both in vitro and in vivo, and the underlying mechanisms were also investigated.

RESULTS AND DISCUSSION

Preparation and Characterization of Three-Functional Platinum(IV) Conjugates. The three-functional platinum (IV) complexes **1**−**2** containing CTP-ASP ligands were synthesized according to the procedures outlined in Scheme 1. The CTP-ASP acid **6** was prepared using ASP and CTP as starting materials, while oxoplatin **7** was obtained by

https://doi.org/10.1021/acs.jmedchem.5c00815
J. Med. Chem. 2025, 68, 11928−11947

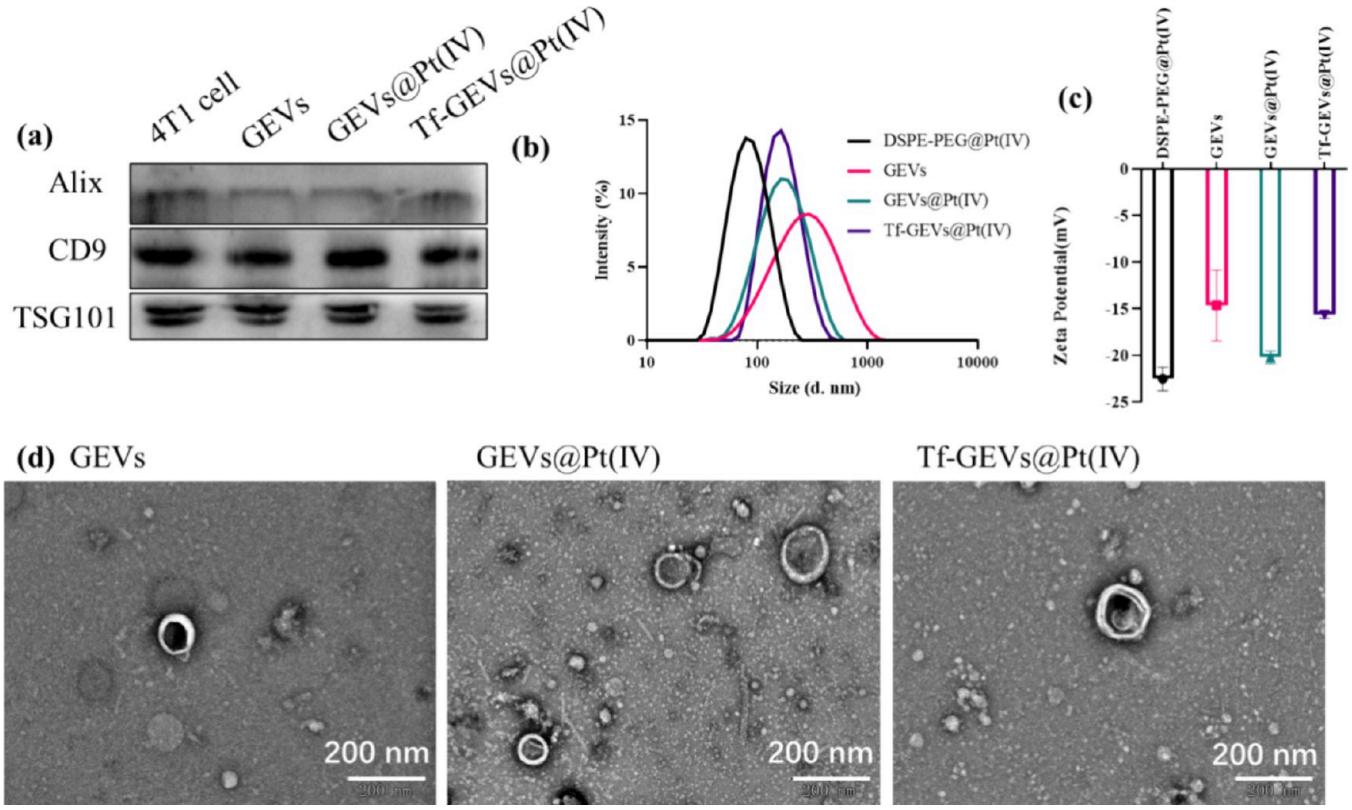

Figure 2. Characterization of DSPE-PEG@Pt(IV), GEVs, GEVs@Pt(IV), and Tf-GEVs@Pt(IV) was performed using Western blot, DLS, and TEM assays. (a) Western blot analysis of the marker proteins Alix, CD9, and TSG101. (b, c) Size distribution and zeta potential determined by DLS. (d) TEM images of nanoparticles.

oxidizing CDDP with hydrogen peroxide. The condensation of oxoplatin **7** with acid **6** in a ratio of 1:3 afforded the dual ligand platinum(IV) conjugate **1** with a yield of 32%, in the presence of N,N,N′,N′-tetramethyl-O-(benzotriazol-1-yl)uronium tetrafluoroborate (TBTU) and triethylamine (TEA). Meanwhile, the mono ligand complex **2** was prepared in a yield of 28% starting from compounds **7** and **6** in a ratio of 1:1.2. The dual functional conjugates **3** and **4** were synthesized by the condensation of oxoplatin **7** with acetyl CTP **8** and ASP anhydride **9** in yields of 37 and 35%. The purity of conjugates **1**−**4** was determined by high-performance liquid chromatography (HPLC) assay, and all compounds were >95% pure. Their structures were confirmed by ^{1}H NMR, ^{13}C NMR, ESI-MS, and HRMS spectra.

Preparation and Characterization of Nanoparticles. The antitumor activities of three-functional platinum(IV) conjugates **1** and **2** were assessed primarily using the MTT assay before the preparation of nanoparticles. It was found that the platinum(IV) hybrid **1** bearing dual CTP-ASP ligands exhibited superior antitumor activities compared to the monoligand complex **2** (see the Antiproliferative Activities In Vitro section). Thereby, the nanodrugs were prepared with conjugate **1** as the active ingredient. The platinum(IV) complexes usually undergo reduction easily in a reducing microenvironment; thus, complex **1** was encapsulated in DSPE-PEG_{2000} to produce DSPE-PEG@Pt(IV) before further encapsulation with GEVs to prevent reduction reactions that may occur in exosomes. Then, the DSPE-PEG@Pt(IV) was further wrapped in GEVs under ultrasonication, and the nanomedicine GEVs@Pt(IV) was generated. As determined by atomic absorption spectrometry (AAS), the encapsulation efficiency of conjugate **1** was approximately 94%, suggesting that complex **1** was nearly entirely entrapped within the nanoparticles GEVs@Pt(IV). Subsequently, tumor-targeting nanoparticles Tf-GEVs@Pt(IV) were achieved through the coincubation of DSPE-PEG_{2000}-Tf with GEVs@Pt(IV). A Western blot assay was used to detect the marker proteins of EVs (Figure 2a). It was indicated that GEVs were enriched in Alix, CD9, and TSG101, while nanomedicines GEVs@Pt(IV) and Tf-GEVs@Pt(IV) exhibited similar expression levels of these proteins. These findings suggested that the incorporation of DSPE-PEG@Pt(IV) had a negligible influence on the biological properties of the GEVs.

The nanoparticles were characterized by dynamic laser light scattering (DLS) and transmission electron microscopy (TEM, Figure 2b−d). The size of DSPE-PEG@Pt(IV) was 68.1 ± 0.4 nm (PDI = 0.16 ± 0.01, ζ = −22.54 ± 1.26). The GEVs had larger size of 223.8 ± 5.2 nm (PDI = 0.33 ± 0.03, ζ = −14.64 ± 3.81) than the DSPE-PEG@Pt(IV), which allowed the encapsulation of DSPE-PEG@Pt(IV). Then, GEVs@Pt(IV) and Tf-GEVs@Pt(IV) showed sizes of 146.0 ± 1.9 nm (PDI = 0.27 ± 0.04, ζ = −20.22 ± 0.69) and 190.3 ± 6.3 nm (PDI = 0.39 ± 0.06, ζ = −15.64 ± 0.40), respectively. The morphology reflected by the TEM images further demonstrated a typical well-rounded vesicle structure of the GEVs as reported in the literature.[37] The derived nanoparticles GEVs@Pt(IV) and Tf-GEVs@Pt(IV) were also approximately spherical in shape, with contents, which were ascribed to the embedding of DSPE-PEG@Pt(IV). Then, relatively smaller particle sizes of these nanoparticles were observed in the TEM images, which were ascribed to the dehydration and wrinkling

https://doi.org/10.1021/acs.jmedchem.5c00815
J. Med. Chem. 2025, 68, 11928−11947

Table 1. Antiproliferative Activities of Platinum(IV) Complexes 1−4 and the Nanoparticles GEVs@Pt(IV) and Tf-GEVs@Pt(IV) against Four Tumor Cell Lines with CDDP, the Mixture of CDDP+6, CTP-ASP Acid 6, ASP, and CTP As Reference Drugs[a]

compd.	4T1	A549	A549R	RF[b]	HepG2	LO2	SI[c]
1	2.98 ± 0.20	1.64 ± 0.20	2.36 ± 0.29	1.44	4.18 ± 0.24	9.23 ± 0.39	2.21
2	5.22 ± 0.67	1.14 ± 0.23	4.31 ± 0.25	3.78	18.08 ± 2.80	15.83 ± 1.23	0.88
3	12.92 ± 1.46	11.85 ± 2.18	18.65 ± 2.61	1.57	13.85 ± 0.94	19.46 ± 4.74	1.41
4	2.67 ± 0.59	7.22 ± 1.71	7.58 ± 1.49	1.05	1.86 ± 0.20	4.09 ± 0.45	2.20
GEVs	>50	>50	>50	ND[d]	>50	>50	ND
GEVs@Pt(IV)	3.81 ± 0.56	3.12 ± 0.20	5.89 ± 0.76	1.89	3.39 ± 0.11	8.90 ± 1.22	2.63
Tf-GEVs@Pt(IV)	0.82 ± 0.27	0.84 ± 0.17	0.59 ± 0.16	0.70	1.35 ± 0.15	9.29 ± 1.36	6.88
CDDP	3.86 ± 0.17	3.91 ± 0.51	23.79 ± 1.76	6.08	15.43 ± 1.23	25.98 ± 2.42	1.68
CDDP+**6**[e]	10.04 ± 0.43	4.71 ± 0.56	23.83 ± 1.80	5.06	16.11 ± 1.76	28.56 ± 0.62	1.77
6	55.64 ± 8.12	30.03 ± 5.56	>50	ND	25.89 ± 3.00	>50	ND
ASP	>50	>50	>50	ND	>50	>50	ND
CTP	>50	>50	>50	ND	>50	>50	ND

[a]Cells were treated by drugs for 48 h, and the half maximal inhibitory concentration (IC_{50}, μM) was given based on three parallel experiments. [b]RF, resistant factor; RF = IC_{50}(A549R)/IC_{50}(A549). [c]SI, selectivity index; SI = IC_{50}(LO2)/IC_{50}(HepG2). [d]ND, not tested or not calculated. [e]CDDP+**6**: a mixture of CDDP and acid **6** with a molar ratio of 1:2.

of the nanoparticles during the preparation of the TEM samples.

The stability investigation in Figure S1 revealed that the size of GEVs and nanodrug GEVs@Pt(IV) remained stable during the 7 days of incubation, while GEVs@Pt(IV) and Tf-GEVs@Pt(IV) were also stable. These facts indicated that the nanomedicines with GEVs as vehicles embedding DSPE-PEG@Pt(IV) were stable in an aqueous medium.

Release Behavior of Complex 1 from Nanoparticles. The release behavior of the active ingredient from the nanoparticles dramatically influences their antitumor activities. Herein, the release of active ingredient **1** from the nanodrugs GEVs@Pt(IV) and Tf-GEVs@Pt(IV) was conducted in PBS media, with an injection of free complex **1** (dissolved in PBS containing 5% DMF) as a reference (Figure S2). It was demonstrated that both GEVs@Pt(IV) and Tf-GEVs@Pt(IV) could release conjugate **1** gradually for about 80% in 24 h; meanwhile, the free complex **1** injection was released in a burst manner (up to 88% within the initial 6 h). As a result of the long-term drug release behavior of these nanodrugs, tumor cells were allowed to be exposed to chemotherapeutics for a prolonged period, which would further enhance the antitumor activities. The platinum(IV) conjugates as prodrugs of platinum(II) drugs usually possess better stability than their precursors, which would prevent the inactivation caused by the sulfur-containing biomolecules, further reduce toxicity, and improve antitumor activities. Herein, the stability of complex **1** in biological media was evaluated in RPMI 1640, which was often used as a model of biological media. The HPLC spectra in Figure S3 reflected that complex **1** mainly remained stable for at least 24 h in RPMI 1640.

Overall, the nanodrugs GEVs@Pt(IV) and Tf-GEVs@Pt(IV) could release the active ingredient complex **1** in a slow and sustained manner, which would remain stable in biological media.

Antiproliferative Activities In Vitro. The antitumor activities of the platinum(IV) complexes **1**−**4** and the nanoparticles GEVs@Pt(IV) and Tf-GEVs@Pt(IV) were evaluated using the MTT assay against four tumor cell lines including human lung cancer (A549), CDDP resistant human lung cancer (A549R), murine breast cancer (4T1), and human liver cancer (HepG2), and one normal human liver cell line (LO2), while CDDP, the mixture of CDDP+**6**, acid **6**, ASP, and CTP were applied as reference drugs (Table 1).

The ligand displayed a remarkable influence on antitumor performance. The three-functional complex **1** with CTP-ASP ligands was obviously more effective than the corresponding dual-functional complexes **3** and **4** with CTP or ASP ligands, which was probably ascribed to its three-functional action mode. Then, complex **2** with mono ligand exhibited significantly lower activity than the dual ligand complex **1**, mainly due to the impacts of uptake, as conjugate **1** resulted in improved platinum accumulation levels in tumor cells compared to conjugate **2** ($P < 0.001$, Figure S4). Consequently, conjugate **1** displayed the most potent antitumor activity against all the tested tumor cell lines with IC_{50} values lower than 4.18 μM, which was significantly more potent than the references CDDP, acid **6**, and the mixture of CDDP+**6**. Accordingly, conjugate **1** was selected as a candidate for further preparation of the nanodrugs.

The GEV-derived nanoparticles GEVs@Pt(IV) and Tf-GEVs@Pt(IV), embedding complex **1** as an active ingredient, also exhibited potent antitumor performance. Especially, Tf-GEVs@Pt(IV) with the tumor targeting motif Tf displayed over 1.9-fold more potent activities than free complex **1** against all tumor cell lines. The accumulation of drugs in tumor cells has been recognized as a pivotal factor influencing antitumor efficacy, especially for platinum-based drugs. Herein, the uptake levels in 4T1 cells were evaluated (Figure S4). It was realized that the incorporation of motif Tf significantly enhanced the drug accumulation of Tf-GEVs@Pt(IV) in tumor cells, in contrast to GEVs@Pt(IV) ($P < 0.001$) and free complex **1** ($P < 0.001$), which served as a key factor contributing to its improved antitumor performance.

Drug resistance has long been a clinical conundrum in cancer treatment with platinum drugs. Herein, the resistant factor (RF) as a ratio of the IC_{50} value for A549R to that of A549 was calculated to determine the potency of these drugs in overcoming drug resistance. It was realized that all of the prepared platinum(IV) conjugates were potent in reducing drug resistance with lower RF values (1.05−3.78) than the reference drug CDDP (RF = 6.08) and the mixture of CDDP+**6** (RF = 5.06). Then, the nanodrugs GEVs@Pt(IV) and Tf-GEVs@Pt(IV) also possessed rather reduced RF = 1.89 and

https://doi.org/10.1021/acs.jmedchem.5c00815
J. Med. Chem. 2025, 68, 11928−11947

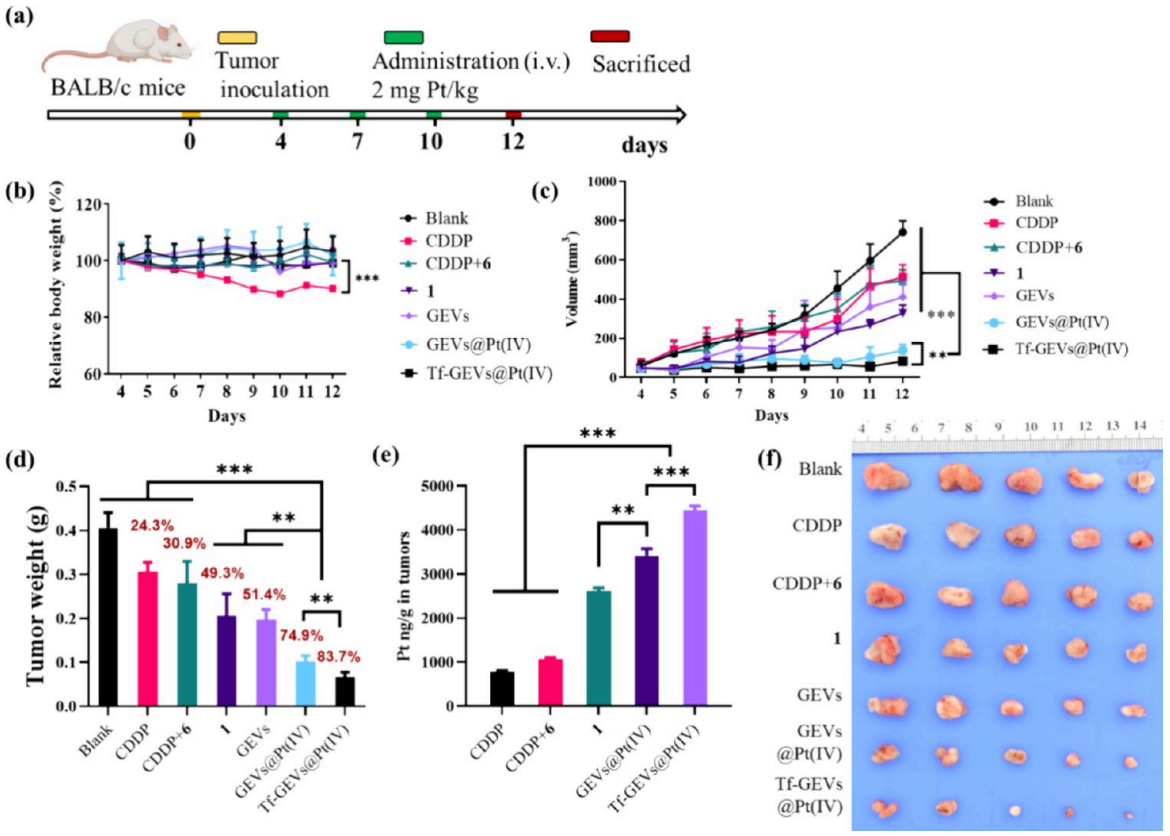

Figure 3. In vivo antitumor activities of candidate platinum(IV) complex **1**, and the nanoparticles GEVs@Pt(IV) and Tf-GEVs@Pt(IV) against 4T1 tumors in female BALB/c mice, with GEVs, CDDP, and a mixture of CDDP+**6** as reference drugs (n = 5). (a) Schematic illustration of the experimental design. (b) Relative body weight of the mice during the treatment. (c) Tumor growth as a function of time. (d) Tumor weight of each group at the end of the experiment. The TGI of the tested drugs in comparison with the blank group was depicted above the column [TGI = (1 − tumor weight of the drug-treated group/tumor weight of blank group) × 100%]. (e) Platinum accumulation in tumor tissues. (f) Image of tumors at the end of the experiment. $^{**}P < 0.01$, $^{***}P < 0.001$.

0.70, indicating their great potential in overcoming the drug resistance of CDDP.

The serious toxicity to normal cells is another barrier to the clinical use of platinum drugs. The selective index (SI) as a ratio of the IC_{50} value for LO2 to that of HepG2 was also calculated. Candidate conjugate **1** could decrease toxicities to some extent by improving the SI value to 2.21 in comparison with CDDP (SI = 1.68) and the mixture of CDDP+**6** (SI = 1.77). Notably, the nanomedicine Tf-GEVs@Pt(IV) possessed a dramatically higher SI = 6.88 than the free complex **1** and GEVs@Pt(IV) (SI = 2.21, 2.63), which was probably ascribed to the elevated tumor targeting properties.

Accordingly, nanodrugs derived from GEVs loaded with three-functional platinum(IV) conjugates represent a promising platform for the exploration of anticancer drugs. Complex **1** bearing dual CTP-ASP ligands displayed improved antitumor activities in comparison with the reference drug CDDP and the mixture of CDDP+**6**. The construction of nanomedicines with GEVs loading complex **1** further enhanced the antitumor performance. In particular, Tf-GEVs@Pt(IV) with the tumor-targeting motif Tf exhibited the most significant antitumor potency and demonstrated great potential in overcoming drug resistance and reducing the toxicities associated with platinum drugs. The in vivo antitumor activities and mechanisms were further investigated in the following experiments.

Inhibition to Tumor Growth In Vivo. To determine the antitumor activities in vivo, the female BALB/c mice were employed to establish 4T1 tumor xenograft animal models by inoculating 1×10^6 cells subcutaneously per mouse in the left flank. The candidate complex **1**, and nanodrugs GEVs@Pt(IV) and Tf-GEVs@Pt(IV) were intravenously administered (i.v.) at a dose of 2 mg of Pt/kg at three-day intervals, three times with GEVs (same amount as in nanodrugs), CDDP, and the mixture of CDDP+**6** (1:2) as reference drugs (Figure 3a).

The candidate complex **1** led to a more effective suppression of tumor growth in vivo than the reference drug CDDP and the mixture of CDDP+**6**, the trend of which was similar to the MTT results in vitro (Figure 3c,d). Then, the nanodrugs GEVs@Pt(IV) and Tf-GEVs@Pt(IV) were significantly more potent than complex **1** ($P < 0.01$). Notably, the GEVs also exhibited moderate anti-growth ability against tumors with a TGI = 51.4%, demonstrating their function as more than just simple carriers of the active ingredient, which further contributed to the enhanced antitumor activities of the nanomedicines. Furthermore, the Tf modified nanodrug Tf-GEVs@Pt(IV) displayed the most promising antitumor competence, and resulted in smaller tumor volume (85.5 mm^3) and higher TGI (83.7%) than GEVs@Pt(IV) (138.3 mm^3, 74.9%, $P < 0.01$). To further detect the underlying mechanism for these effective antitumor agents, the histology analysis was conducted based on the hematoxylin and eosin (H&E) staining results. The images in the manifest showed that considerable apoptotic and necrotic regions were observed in tumors of conjugate **1**, GEVs@Pt(IV), and Tf-GEVs@

https://doi.org/10.1021/acs.jmedchem.5c00815
J. Med. Chem. 2025, 68, 11928−11947

Pt(IV)-treated groups, which were even more significant than those of the CDDP and CDDP+**6** groups. These facts disclosed that the encapsulation of three-functional platinum(IV) conjugate **1** into GEVs to prepare the corresponding nanoparticles was effective in improving the antitumor activities in vivo.

The accumulation of chemotherapeutic agents in tumors has been regarded as a pivotal factor influencing antitumor efficacy. Herein, the platinum accumulation in tumor tissues was measured using atomic absorption spectroscopy (AAS) assay. The drug accumulation data in Figure 3e were mainly in tune with the antitumor potency of the drugs that complex **1** and the nanomedicines GEVs@Pt(IV) and Tf-GEVs@Pt(IV) accumulated in tumors at remarkably higher levels than CDDP and CDDP+**6** ($P < 0.01$ or $P < 0.001$). Especially, Tf-GEVs@Pt(IV) accumulated in tumors more easily than free complex **1** and GEVs@Pt(IV) ($P < 0.001$), which was mainly ascribed to the tumor targeting properties. These facts demonstrated that drug accumulation in tumors displayed great impacts on the antitumor activities of the title nanodrugs based on the three-functional platinum(IV) conjugates in vivo.

The in vivo taxic properties demonstrated by the change of body weight during the experiment (Figure 3b) and the H&E staining results (Figure S5) disclosed that complex **1** and its nanoparticles GEVs@Pt(IV) and Tf-GEVs@Pt(IV) caused no obvious toxicities in vivo. No significant body weight loss of mice was caused by these drugs in comparison with the blank group, which was less toxic than CDDP ($P < 0.001$). No significant histological differences were observed in the liver, spleen, and kidney tissues. Notably, the combination of CDDP+**6** also exhibited less toxicity than free CDDP, indicating that the functional moieties ASP and CTP in acid **6** probably participated in reducing the toxic effects of the platinum drugs, which further served as a factor contributing to the low toxicity of platinum(IV) hybrid **1** and its nanomedicines.

Accordingly, the construction of a three-functional platinum(IV) complex **1** by incorporating a CTP-ASP ligand led to a remarkable increase in antitumor potency and a reduction of toxicity in vivo. Then, the preparation of nanodrug Tf-GEVs@Pt(IV), using GEVs as vehicles and Tf as a tumor-targeting motif, further improved the accumulation of platinum active ingredient **1** in tumors and enhanced the antitumor efficacy.

Inhibition to Metastatic Tumors In Vitro and In Vivo. The development of novel antitumor drugs with potent antimetastatic activities has aroused abundant attention, which is of great potential in increasing the survival rate of cancer patients. Herein, the inhibition of metastatic tumors of candidate platinum(IV) complex **1** and the nanodrugs GEVs@Pt(IV) and Tf-GEVs@Pt(IV) were evaluated both in vitro and in vivo.

The transwell experiment indicated that complex **1** could effectively inhibit the migration of tumor cells in vitro, which was obviously more potent than GEVs, CDDP, and CDDP+**6** ($P < 0.001$) (Figure S6). Then, the conversion of this candidate into nanodrugs GEVs@Pt(IV) and Tf-GEVs@Pt(IV) further increased the antimetastatic properties ($P < 0.001$). Then, their antimetastatic potency was further verified by the wound-healing assay (Figure S7) in which platinum(IV) complex **1**, GEVs@Pt(IV), and Tf-GEVs@Pt(IV) suppressed the wound-healing of tumor cells effectively in comparison with the blank, CDDP, CDDP+**6**, and GEVs groups. These facts proved that the three-functional platinum(IV) complex **1**, as well as its nanomedicines GEVs@Pt(IV) and Tf-GEVs@Pt(IV), were potent in inhibiting the metastasis of tumor cells in vitro.

The lung is the primary site of tumor metastasis. Consequently, the activities against metastatic tumors were assessed using pulmonary metastasis models in female BALB/c mice (Figure 4). The candidate complex **1**, and the

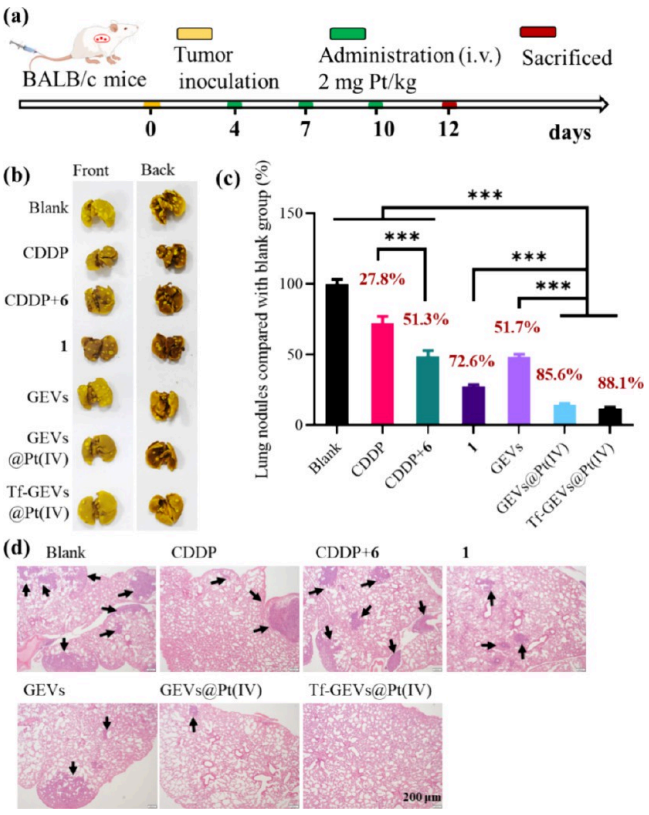

Figure 4. Pulmonary metastasis inhibition properties of complex **1** and the nanoparticles GEVs@Pt(IV) and Tf-GEVs@Pt(IV) against 4T1 tumors in female BALB/c mice with GEVs, CDDP, and the mixture of CDDP+**6** as reference drugs ($n = 5$). ***$P < 0.001$. (a) Schematic illustration of the experimental design. (b) Representative photographs of front and back sides of lungs from each group at the end of the experiment. (c) Lung nodules in each group. The inhibition rate in comparison with the blank group was depicted above the column. (d) H&E staining of lung metastasis nodules. Nodules were indicated by arrows.

nanoparticles GEVs@Pt(IV) and Tf-GEVs@Pt(IV) were administered at a dosage of 2 mg of Pt/kg on days 4, 7, and 10, with CDDP, the mixture of CDDP+**6**, and GEVs (same concentration as in the nanodrugs) as reference groups. In tune with the results in vitro, complex **1**, GEVs@Pt(IV), and Tf-GEVs@Pt(IV) displayed remarkable suppression against the 4T1 pulmonary metastatic tumors in vivo. Notably, platinum(IV) candidate complex **1** possessed superior activities in comparison with CDDP and the mixture of CDDP+**6**, indicating that the incorporation of functional ligand CTP-ASP into the platinum(IV) system was pivotal in improving the inhibitory performance against metastatic tumors. Moreover, the GEVs demonstrated significant competence in inhibiting tumor metastasis in vivo (51.7%), manifesting that GEVs not only served as carriers for active ingredient **1** but also participated in the suppression of metastatic tumors, further contributing to the superior

https://doi.org/10.1021/acs.jmedchem.5c00815
J. Med. Chem. 2025, 68, 11928−11947

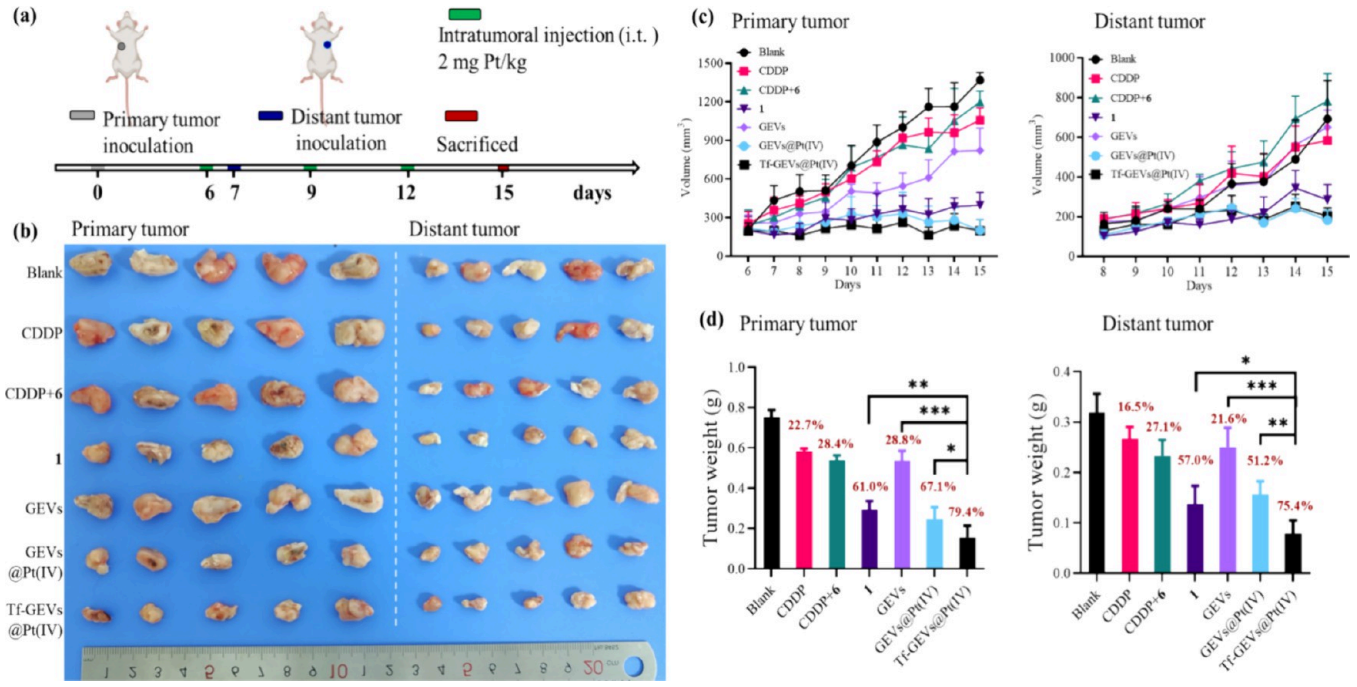

Figure 5. Antitumor immunity of candidate platinum(IV) complex **1** and the nanoparticles GEVs@Pt(IV) and Tf-GEVs@Pt(IV) in BALB/c mice bearing bilateral 4T1 tumors in vivo (n = 5) with GEVs, CDDP, and the mixture of CDDP+**6** as reference drugs. (a) Schematic illustration of the experimental design. (b) Image of tumors at the end of the therapeutic period. (c) Volume of primary and distant tumors as a function of time. (d) Weight of primary and distant tumors at the end of the experiment. *P < 0.05, **P < 0.01, ***P < 0.001.

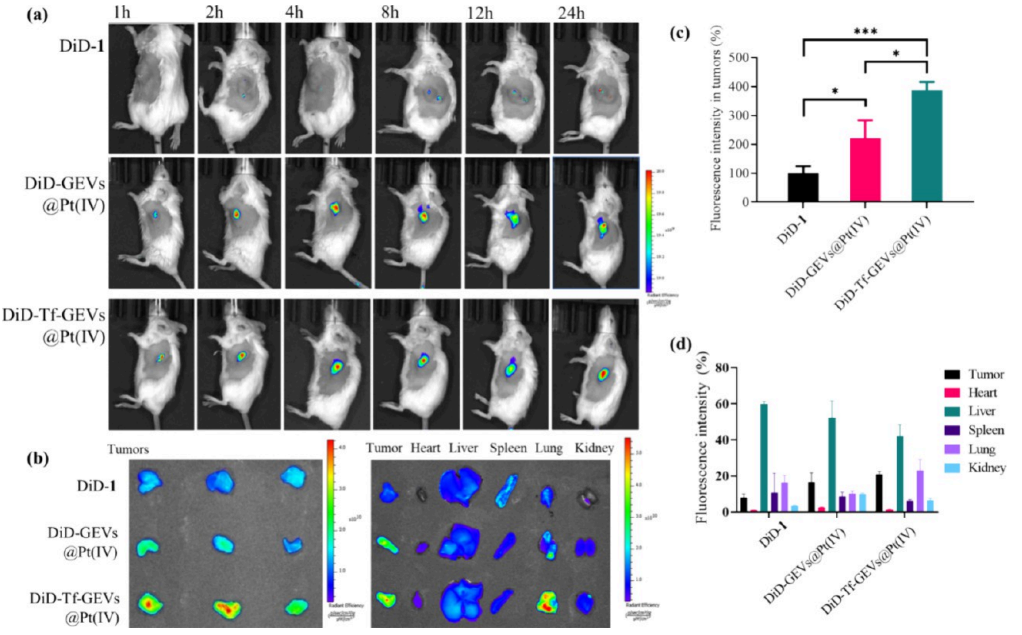

Figure 6. Biodistribution and targeting study of DiD-labeled nanoparticles DiD-GEVs@Pt(IV) and DiD-Tf-GEVs@Pt(IV), and the mixture of DiD with free complex **1** (DiD-**1**) in vivo (n = 3). (a) Mice bearing 4T1 tumor grafts were injected (i.v.) with the DiD-labeled agents followed by dynamic scanning using an IVIS optical imaging system at 1, 2, 4, 8, 12, and 24 h postinjection. (b) Ex vivo images of the tumors and tissues including heart, liver, spleen, lung, and kidney. (c) The relative fluorescence intensity in tumors at the end of the experiment. (d) The distribution of drugs in tissues (Relative fluorescence intensity = (Fluorescence intensity in specified tissues/Fluorescence intensity in all tissues including tumor, heart, liver, spleen, lung and kidney) × 100%). *P < 0.05, ***P < 0.001.

performance of the nanomedicines. Furthermore, nanodrugs GEVs@Pt(IV) (85.6%) and Tf-GEVs@Pt(IV) (88.1%) exerted more pronounced activities than the free complex **1** (72.6%, P < 0.001) in vivo, which revealed that the GEV-derived nanodrugs loaded with three-functional platinum(IV) conjugates represented a promising platform for developing novel drugs against metastatic tumors.

Activating Antitumor Immunity In Vivo. The three-functional platinum(IV) conjugates with CTP-ASP ligands were exposed to active antitumor immunity in vivo. The effects of immunity on the antitumor competence were detected using

https://doi.org/10.1021/acs.jmedchem.5c00815
J. Med. Chem. 2025, 68, 11928−11947

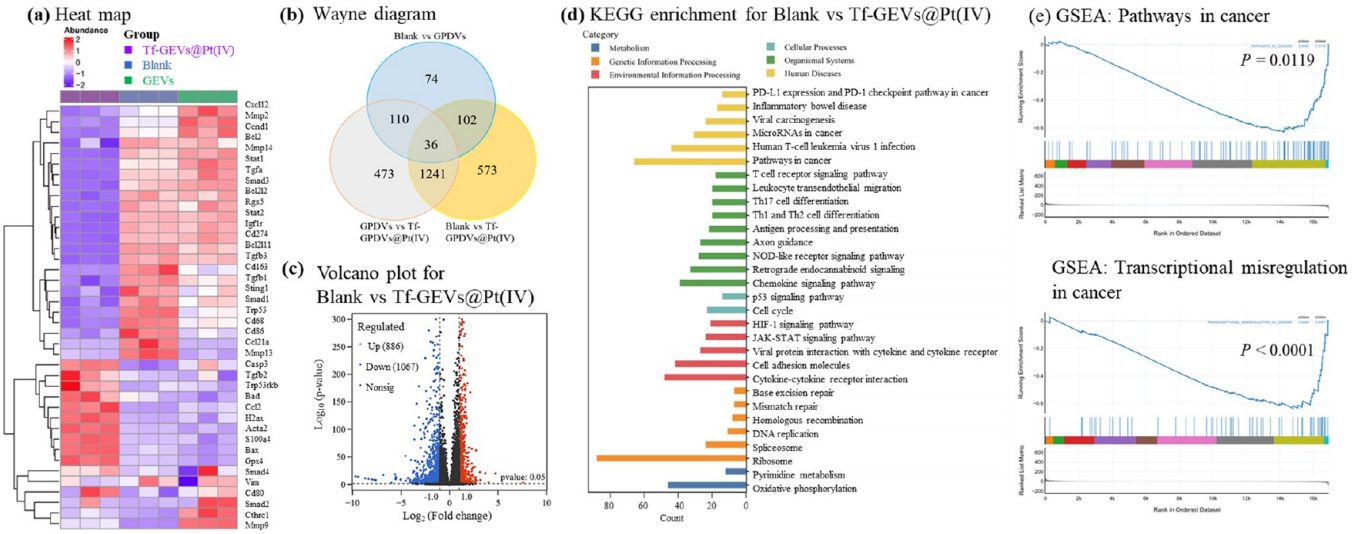

Figure 7. RNA-seq analysis of 4T1 tumor tissues from the blank, GEVs, and Tf-GEVs@Pt(IV) treated groups of the antitumor growth experiments. (a) Heatmap of the main genes. (b) Wayne diagram of DEGs in three groups. (c) Volcano plot of DEGs for blank vs Tf-GEVs@Pt(IV) groups. (d) KEGG enrichment for blank vs and Tf-GEVs@Pt(IV). (e) GSEA analysis for blank vs and Tf-GEVs@Pt(IV).

bilateral homogenotypic 4T1 tumor models on the immunocompetent female BALB/c mice (Figure 5a), where the primary tumor was inoculated in the left flank of mice on day 0, and the distant tumor in the right flank on day 7 (n = 5). Then, the candidate complex **1**, and the nanoparticles GEVs@Pt(IV) and Tf-GEVs@Pt(IV) were intratumorally injected (i.t., 2 mg of Pt/kg) on days 6, 9, and 12, with CDDP, the mixture of CDDP+**6**, and GEVs (same concentration as in the nanodrugs) as reference groups. The volume of both tumors was monitored throughout the experiment. The mice were sacrificed on day 15, and the TGI was calculated based on the tumor weight.

As shown in Figure 5b−d, the tumor targeted nanomedicine Tf-GEVs@Pt(IV) could inhibit the growth of primary tumors by 79.4% compared with the blank group, which was significantly superior to GEVs@Pt(IV) (67.1%, $P < 0.05$), free conjugate **1** (60.1%, $P < 0.01$), and the vehicle GEVs (21.6%, $P < 0.001$), while the platinum(II) references CDDP and CDDP+**6** only inhibited the growth of the primary tumors by 22.7 and 28.4%. These facts further verified the promising antigrowth properties of three-functional platinum(IV) hybrid **1** and its GEV-derived nanodrugs in vivo. More importantly, the untreated distant tumors were also suppressed, primarily due to the antitumor immunity elicited by the drugs in vivo. Complex **1**, GEVs@Pt(IV), and Tf-GEVs@Pt(IV) led to high inhibition rates against the distant tumors, ranging from 51.2 to 75.4%, but CDDP and CDDP+**6** caused rather lower inhibition rates of 16.5 and 27.1%. Moreover, Tf-GEVs@Pt(IV) with the most potent antitumor potency in vivo also exhibited the most promising potency in initiating antitumor immunity with the highest TGI = 75.4% against the distant tumors, which was superior to GEVs@Pt(IV) (TGI = 51.2%, $P < 0.01$) and conjugate **1** (TGI = 57.0%, $P < 0.05$), indicating that the tumor targeting properties also effectively influenced the promotion of immunity in tumors. Thus, the three-functional platinum(IV) complexes designed in this work could modulate antitumor immunity in vivo, especially the nanomedicines, which further elevated their potential in promoting immune responses.

Tumor Targeting and Biodistribution Study In Vivo. The incorporation of Tf motifs onto the nanoparticles was expected to improve the tumor-targeting properties of nanodrugs by binding to overexpressed TfR on the surface of tumor cells, thereby contributing to superior antitumor activity. The lipophilic dye DiD is commonly used in the tumor targeting investigation of nanodrugs. In this study, the tumor-targeting properties of DiD-Tf-GEVs@Pt(IV) and DiD-GEVs@Pt(IV) were assessed in 4T1-bearing female BALB/c mice, using DiD as a probe and a mixture of complex **1** with DiD (DiD-**1**) as a reference drug.

The results shown in Figure 6a indicated that the fluorescence signal of the DiD-GEVs@Pt(IV) and Tf-DiD-GEVs@Pt(IV) groups improved gradually with the extension of treatment time and was significantly higher than that of the DiD-**1**. These findings proved that the nanodrugs derived from GEVs accumulated in tumor tissues at higher levels than those of free complex **1**, which was mainly attributed to the enhanced penetration effects of GEVs and the enhanced permeability and retention (EPR) effects. Then, the mice were sacrificed at 24 h, and the biodistribution of drugs in tumors and organs, including the heart, liver, spleen, lung, and kidney, was evaluated by the IVIS spectrum. As shown in Figure 6b−d, the fluorescence intensity of DiD-Tf-GEVs@Pt(IV) group was relatively higher than that of the DiD-GEVs@Pt(IV) group ($P < 0.05$), demonstrating that the introduction of Tf ligand was pivotal in improving the tumor targeting properties of nanodrugs in vivo. More encouragingly, a higher portion of DiD-Tf-GEVs@Pt(IV) accumulated in the tumors (21.0%) compared to that of the DiD-GEVs@Pt(IV) (16.6%) and DiD-**1** groups (8.1%), which would facilitate its low toxic effects in vivo. The uptake in tumor tissues is additional evidence reflecting the tumor targeting properties directly. The results in Figure 3e also indicated that the drugs accumulated in tumors as a consequence of Tf-GEVs@Pt(IV) > GEVs@Pt(IV) > conjugate **1**. These facts demonstrated that GEVs were promising vehicles for enhancing the penetrating abilities of nanodrugs, while further modification with the Tf motif would improve the tumor-targeting competence of the platinum(IV)

https://doi.org/10.1021/acs.jmedchem.5c00815
J. Med. Chem. 2025, 68, 11928−11947

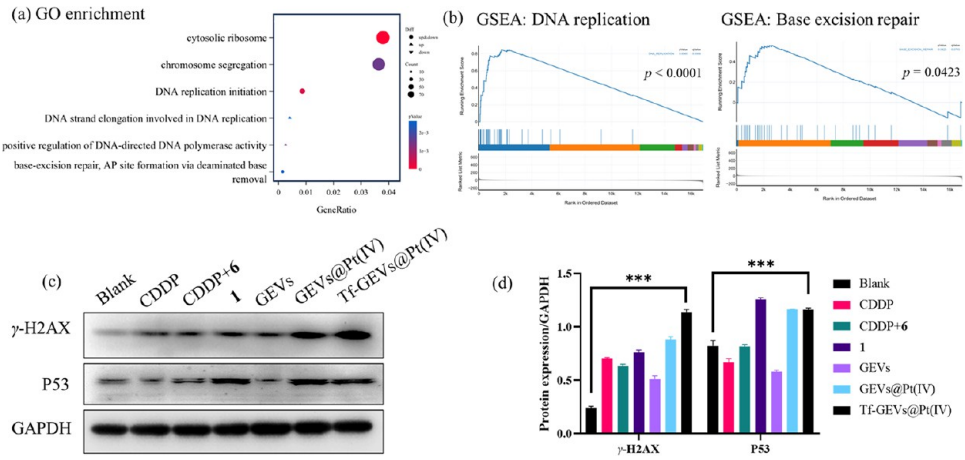

Figure 8. Potency in causing DNA damage. (a, b) GO enrichment and GSEA analysis of the DEGs in blank vs Tf-GEVs@Pt(IV) concerning DNA injury. (c, d) Western blot analysis of γ-H2AX and P53 in 4T1 cells treated for 24 h at 37 °C by CDDP (5 μM), CDDP+**6** (5 μM/10 μM), complex **1** (5 μM), GEVs@Pt(IV) (5 μM), and Tf-GEVs@Pt(IV) (5 μM), with cells treated by PBS and GEVs as controls. ***$P < 0.001$.

conjugates, which further played a significant role in improving antitumor activities and reducing toxicities.

RNA Sequencing Analysis. The RNA-sequencing (RNA-seq) of tumor tissues from the blank, GEVs, and Tf-GEVs@Pt(IV) groups was performed to analyze the underlying antitumor mechanisms (Figures 7 and S8). The Tf-GEVs@Pt(IV) induced abundant differentially expressed genes (DEGs) in tumor cells in comparison with the blank (1952) and GEVs (1860) groups. Moreover, 1241 DEGs appeared simultaneously in the subsets of blank vs Tf-GEVs@Pt(IV) and GEVs vs Tf-GEVs@Pt(IV), demonstrating that the active ingredient, three-functional platinum(IV) conjugate, was essential in causing DEGs in tumors. Subsequently, the Kyoto Encyclopedia of Genes and Genomes (KEGG), Gene Ontology (GO), and Gene Set Enrichment Analysis (GSEA) were conducted to compare blank vs Tf-GEVs@Pt(IV). The DEGs were mainly involved in the regulation of DNA injury and replication, apoptosis, inflammation, tumor cadherin, migration, immunology, and TME information. Thus, an extensive investigation of the mechanisms of the title agent Tf-GEVs@Pt(IV) was further conducted in the following experiments.

Reduction in TME and Causing DNA Damage. DNA damage is the pivotal mechanism by which platinum drugs induce tumor apoptosis. The platinum(IV) complexes are expected to cause serious DNA injury after reduction to the platinum(II) form, which would further bind to the N7-position of guanine. The GO enrichment analysis of the DEGs in tumor tissues indicated that Tf-GEVs@Pt(IV) significantly influenced the cellular component (CC) of the cytosolic ribosome as well as biological processes (BP) such as DNA replication, formation via deaminated base removal, and DNA strand elongation. Meanwhile, the GSEA highlighted that genes concerning DNA replication and base excision repair were significantly affected (Figure 8a,b). These findings suggested that the genes involved in DNA damage were markedly regulated by Tf-GEVs@Pt(IV), which can be primarily attributed to the platinum(IV) component **1**.

The accumulation of platinum drugs in the nucleus would directly influence their DNA damage competence; thus, the subdistribution of the platinum agents in 4T1 cells was measured using the AAS assay (Figure S9). The three-functional platinum(IV) complex **1** and its nanomedicines, GEVs@Pt(IV) and Tf-GEVs@Pt(IV), displayed superior antitumor performance, leading to higher accumulation levels in DNA compared to the reference drug CDDP and the mixture of CDDP+**6** ($P < 0.01$). Furthermore, the nanoparticles modified with the tumor-targeting motif Tf exhibited even greater accumulation in DNA than free complex **1** and nanomedicine GEVs@Pt(IV), which was probably ascribed to the elevated tumor-targeting properties.

As a three-functional molecule, platinum(IV) complex **1** should be reduced to reduce TME and release its three functional fragments, which is crucial for its antitumor activities. Therefore, the reduction potential of complex **1** was tested in a reducing medium of RPMI 1640 with ascorbic acid (AsA, 1 mM, similar to the TME). It was observed that complex **1** underwent easy reduction to divalent form in the reducing microenvironment, as indicated by the decrease in the peak for complex **1** and the increase in the peak for acid **6** (Figures S10−12). Notably, the peak for ASP was also observed with the extension of the incubation time, demonstrating that CPT-ASP acid **6** could be further hydrolyzed to release CTP and ASP in the biological medium. Subsequently, the DNA binding potency was assessed using guanosine-5′-monophosphate (5′-GMP) as a model for a DNA base. A solution of complex **1** was prepared in a reducing medium of RPMI 1640 containing AsA (1 mM) and 5′-GMP (3 mM), and the mixture was monitored by HPLC (Figure S13). It was observed that a platinate GMP peak emerged after 24 h of incubation, indicating that the released platinum(II) counterpart, following the reduction of complex **1**, could effectively bind to DNA. Furthermore, the expression of DNA injury indicators γ-H2AX and P53 was assessed by Western blotting (Figure 8c,d). Complex **1**, GEVs@Pt(IV), and Tf-GEVs@Pt(IV) significantly increased the expression of both γ-H2AX and P53 compared with the blank group ($P < 0.001$), the trend of which was similar to that of the reference drugs CDDP and CDDP+**6**.

Accordingly, the title nanodrug Tf-GEVs@Pt(IV) was effective in inducing DNA damage, which was mainly attributed to the three-functional platinum(IV) candidate **1**. It could be easily reduced to divalent form in tumors and further combine with DNA to modulate the pathways concerning DNA injury and upregulate the expression of γ-H2AX and P53.

https://doi.org/10.1021/acs.jmedchem.5c00815
J. Med. Chem. 2025, 68, 11928−11947

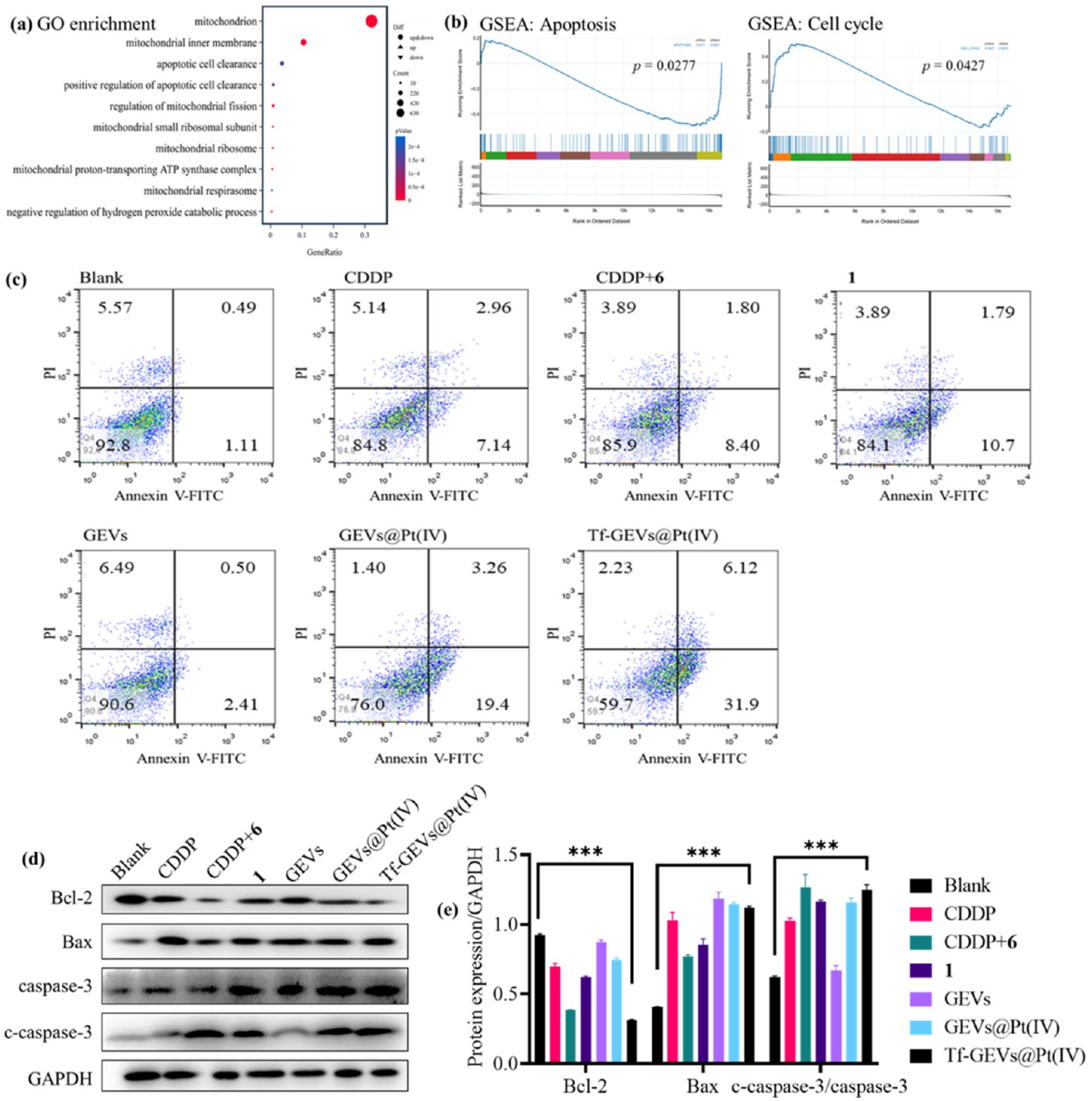

Figure 9. Properties in causing mitochondria-mediated apoptosis. (a, b) GO enrichment and GSEA analysis of the DEGs concerning mitochondria-mediated apoptosis in blank vs Tf-GEVs@Pt(IV). (c) Quantification of apoptosis of 4T1 cells by flow cytometry using an annexin V-FITC/PI staining assay. (d, e) Western blot analysis of Bcl-2, Bax, caspase3, and *c*-caspase-3 in 4T1 cells. The 4T1 tumor cells were incubated for 24 h by CDDP (5 μM), CDDP+**6** (5 μM/10 μM), complex **1** (5 μM), GEVs@Pt(IV) (5 μM), and Tf-GEVs@Pt(IV) (5 μM), with PBS and GEVs as controls. ***$P < 0.001$.

Causing Mitochondria-Mediated Apoptosis. Apoptosis (programmed cell death) is a pivotal mechanism for chemotherapeutics to kill tumor cells and is tightly associated with mitochondrial damage and reactive oxygen species (ROS) generation. Herein, the properties of the prepared agents in inducing mitochondrial-mediated apoptosis were investigated from different aspects.

The GO results indicated that genes concerning positive regulation of apoptotic cell clearance, apoptotic cell clearance (BP), mitochondrion, mitochondrial inner membrane, and mitochondrial ribosome (CC), etc., were modulated in the Tf-GEVs@Pt(IV) treated tumors in comparison with the blank group. While the GSEA also confirmed that pathways associated with apoptosis and cell cycle were ignited (Figure 9a,b). The apoptosis-inducing potency was assessed using the annexin V-FITC/PI staining assay. The results in Figure 9c showed that the nanodrug Tf-GEVs@Pt(IV) aroused a higher percentage of apoptotic cells (38.0%) than the free complex **1** (12.5%) and GEVs@Pt(IV) (22.7%) without Tf ligands, as well as the reference drugs CDDP (10.1%), CDDP+**6** (10.2%),

https://doi.org/10.1021/acs.jmedchem.5c00815
J. Med. Chem. 2025, 68, 11928−11947

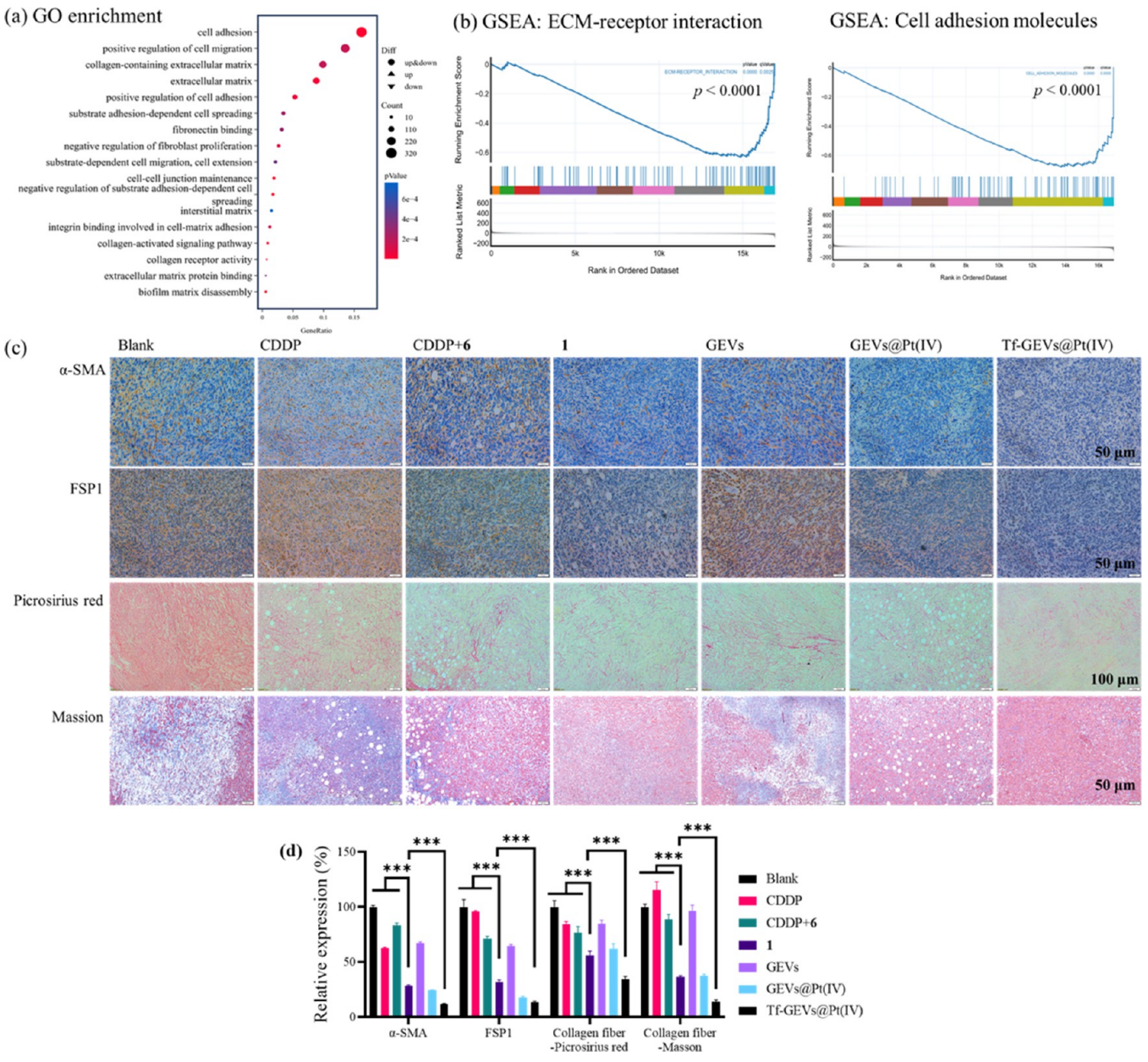

Figure 10. Properties in attenuating the fibrosis of tumors. (a, b) GO enrichment and GSEA analysis of the DEGs in blank vs Tf-GEVs@Pt(IV) concerning fibrosis of tumors. (c, d) Immunohistochemical staining of α-SMA and FSP1, and Picrosirius red, and Masson staining of collagen fiber in tissues from the antitumor experiments in vivo. $^{**}P < 0.01$, $^{***}P < 0.001$.

and GEVs (2.9%). This trend was mainly in tune with the antitumor activities in vitro and in vivo. Then, their potency in damaging mitochondria was further assessed by a JC-1 assay (Figure S14). Serious collapse of mitochondrial membrane potential ($\Delta\Psi_m$) was observed in the Tf-GEVs@Pt(IV) treated tumor cells, which was also superior to that of complex **1**, GEVs@Pt(IV), CDDP, CDDP+**6**, and the GEVs. The ROS generation often served as a driver of apoptosis, accompanied by mitochondrial damage. The DCFH-DA staining assay demonstrated a high level of ROS production in Tf-GEVs@Pt(IV)-treated cells (Figure S15). These facts demonstrated that the title nanomedicine Tf-GEVs@Pt(IV) was effective in causing mitochondria-mediated apoptosis of tumor cells.

The Bcl-2 cascades were regarded as pivotal events in governing the apoptosis process; herein, the expression of proteins in the Bcl-2 pathway was measured by the Western Blotting assay. As observed in Figure 9d,e, the antiapoptotic protein Bcl-2 was significantly downregulated ($P < 0.001$), while the pro-apoptotic protein Bax was upregulated ($P < 0.001$). Additionally, the executive apoptotic protein *c*-caspase-3 was increased, and the ratio of *c*-caspase-3/caspase-3 was significantly elevated compared with the control group ($P < 0.001$). Accordingly, the nanodrug Tf-GEVs@Pt(IV) was potent in inhibiting tumor proliferation by causing apoptosis through the mitochondria-mediated Bcl-2/Bax/caspase-3 signaling in tumors.

Attenuating the Fibrosis in Tumors. Fibrosis of tumors is tightly associated with the ECM, which further influences the adhesion, invasion, migration, and metastasis of tumor cells. The CTP has been proven to be effective in suppressing fibrosis. Herein, the influence of complex **1** with the CTP-ASP

https://doi.org/10.1021/acs.jmedchem.5c00815
J. Med. Chem. 2025, 68, 11928−11947

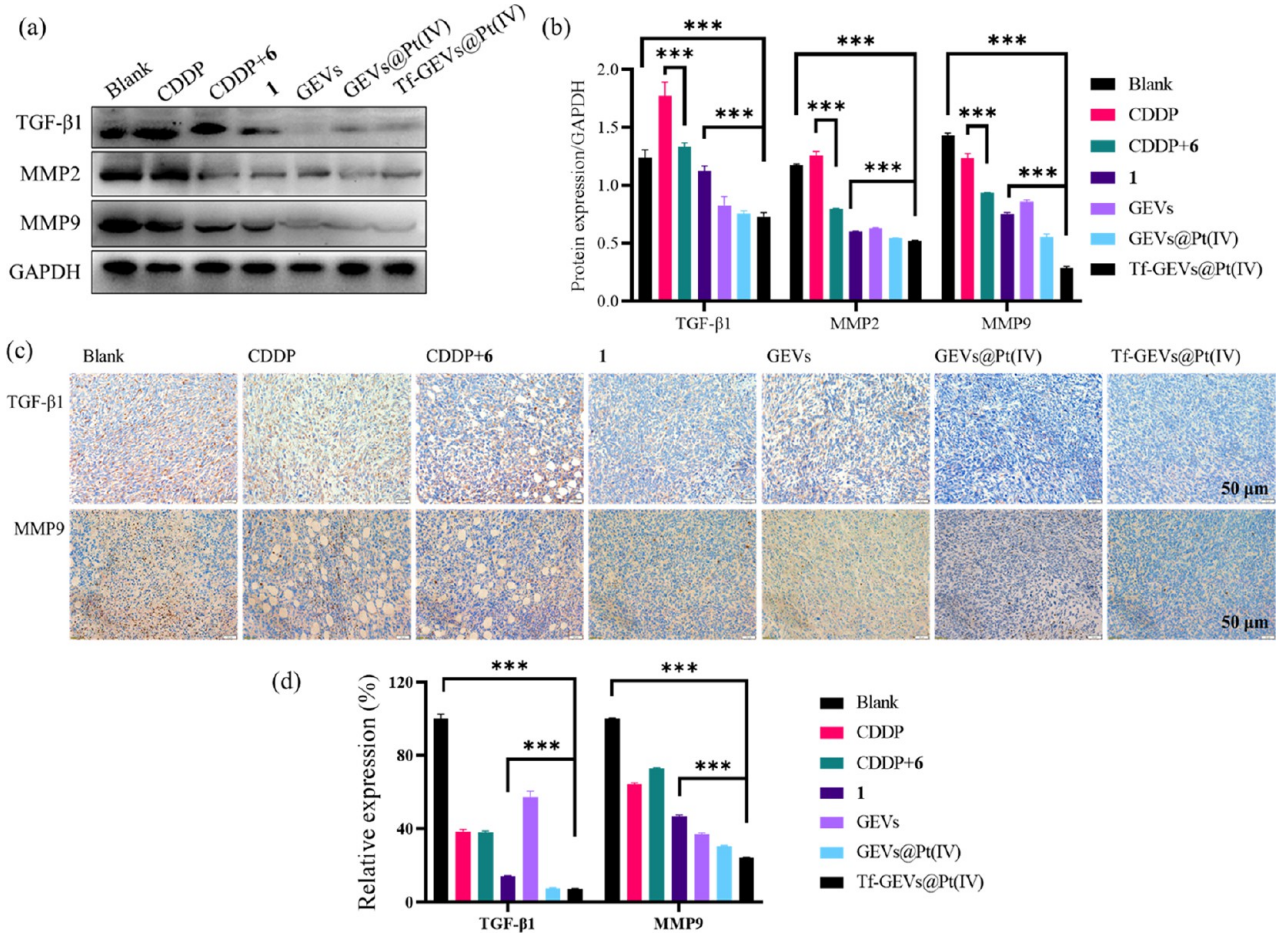

Figure 11. (a, b) Western blot analysis of TGF-β1, MMP2, and MMP9 in 4T1 cells. The 4T1 tumor cells were incubated for 24 h by CDDP (5 μM), CDDP+**6** (5 μM/10 μM), complex **1** (5 μM), GEVs@Pt(IV) (5 μM), and Tf-GEVs@Pt(IV) (5 μM), with PBS and GEVs as controls. (c, d) Immunohistochemical staining of TGF-β1 and MMP9 in tumor tissues from the antitumor experiments in vivo. ***$P < 0.001$.

ligand and nanodrugs GEVs@Pt(IV) and Tf-GEVs@Pt(IV) on the fibrosis of tumors was evaluated.

The GO enrichment showed that the Tf-GEVs@Pt(IV) caused a remarkable change in genes associated with fibrosis, adhesion, and migration of tumor cells; meanwhile, the GSEA analysis demonstrated the involvement of ECM-receptor interaction and cell adhesion molecules in tumors (Figure 10a,b). The Picrosirius red and Masson staining results (Figure 10c,d) manifested that Tf-GEVs@Pt(IV), GEVs@Pt(IV), and complex **1** obviously decreased the levels of collagen fibrosis in tumor slices compared with the blank control group ($P < 0.001$), while the platinum(II) drug had negligible effects. Moreover, the proteins α-SMA and FSP1 associated with collagen fibrosis were also decreased ($P < 0.001$), demonstrating the significant efficacy of complex **1** and its nanodrugs Tf-GEVs@Pt(IV) and GEVs@Pt(IV) in suppressing the tumor fibrosis. Notably, Tf-GEVs@Pt(IV) exhibited the most prominent performance in vivo, which was probably due to its superior tumor targeting capability.

Protein TGF-β is essential for fibrosis induction and activation of the cancer matrix. While MMPs, as pivotal enzymes in modulating the ECM, show crosstalk with TGF-β in tumors, in promoting tumor metastasis and fibrosis. Moreover, CTP is effective in downregulating ECM deposition by blocking the TGF-β1 and MMP pathways. Subsequently, the expression of proteins TGF-β1, MMP2, and MMP9 was evaluated by Western blot and immunohistochemical staining assays. It was realized in Figure 11a,b that the TGF-β1, MMP2, and MMP9 were simultaneously suppressed in the Tf-GEVs@Pt(IV) treated 4T1 cells compared with the blank group ($P < 0.001$), which was more effective than the free complex **1** ($P < 0.001$). While these suppressions were also observed in the tumors from the in vivo antitumor experiment (Figure 11c,d). Interestingly, the mixture of CDDP+**6** also effectively suppressed the secretion of TGF-β1, MMP2, and MMP9 in tumor cells in vitro, compared to CDDP ($P < 0.001$), which was similar to the effects of the three-functional platinum(IV) hybrid **1**. However, this trend was not observed in tumors in vivo. These findings disclosed that conjugate **1** probably displayed a rather distinct action mode in comparison with the mixture of CDDP and the CTP-ASP ligand **6** in vivo.

In this context, the nanomedicine Tf-GEVs@Pt(IV) demonstrated great efficacy in attenuating tumor fibrosis by suppressing key enzymes TGF-β1, MMP2, and MMP9, and it further exhibited promising activities against metastatic tumors both in vitro and in vivo.

Reversing the Inflammatory TME. TAI is a hallmark of cancer and is essential in promoting the formation of a TME, which is strongly associated with tumor fibrosis. TAI is closely linked to upregulation of the key enzyme COX-2 and the secretion of inflammatory cytokines such as TNF-α and IL-6. The incorporation of ASP into three-functional platinum(IV)

https://doi.org/10.1021/acs.jmedchem.5c00815
J. Med. Chem. 2025, 68, 11928−11947

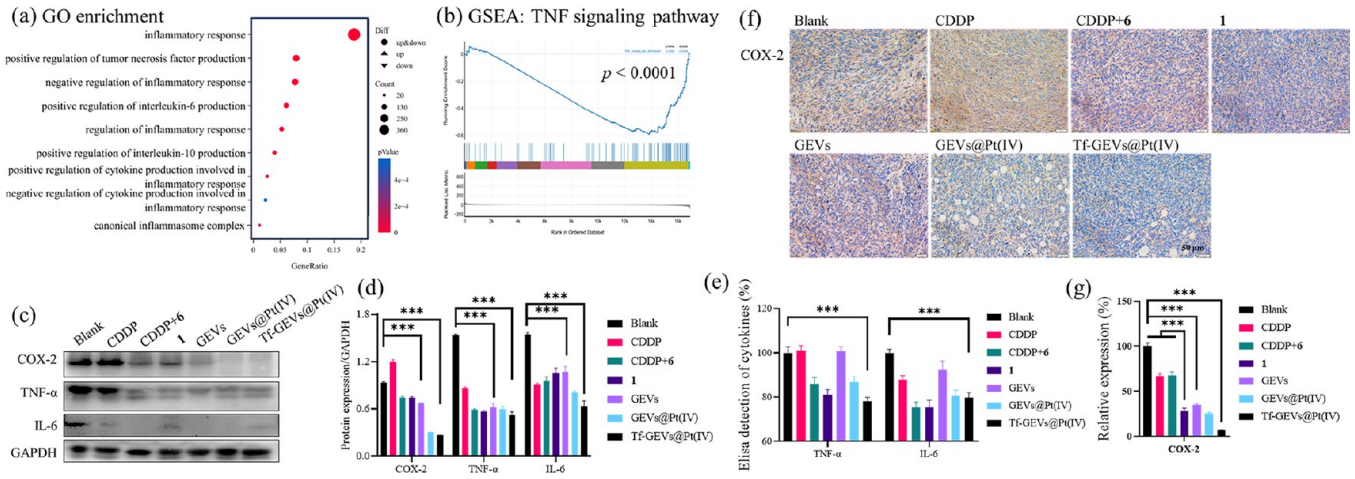

Figure 12. Properties in reversing inflammatory TME. (a, b) GO enrichment and GSEA analysis of the DEGs in blank vs Tf-GEVs@Pt(IV) concerning inflammation. (c, d) Western blot analysis of COX-2, TNF-α, and IL-6 in 4T1 cells. The 4T1 tumor cells were incubated for 24 h with CDDP (5 μM), CDDP+**6** (5 μM/10 μM), complex **1** (5 μM), GEVs@Pt(IV) (5 μM), and Tf-GEVs@Pt(IV) (5 μM), using PBS and GEVs as controls. (e) Elisa analysis of TNF-α and IL-6 in tumor tissues from the antitumor experiments in vivo. (f, g) Immunohistochemical staining of COX-2 in tumor tissues from the antitumor experiments in vivo. ***$P < 0.001$.

conjugates was expected to endow them with anti-inflammatory properties, while the vehicle GEVs were also proven to be potent in inhibiting inflammation. Herein, the effects of the title agents on TAI were investigated.

The KEGG, GO, and GSEA analyses (Figures 7 and 12a,b) based on the RNA-seq data simultaneously demonstrated the influence of Tf-GEVs@Pt(IV) on the inflammatory responses and the cytokine secretion in tumors compared with the blank group. Subsequently, the Western blot and immunohistochemical staining assays (Figure 12c,d,f,g) indicated that the critical enzyme COX-2 was suppressed in Tf-GEVs@Pt(IV) treated tumor cells both in vitro and in vivo ($P < 0.001$). Moreover, the Western blotting and ELISA results further disclosed that the secretion of the cytokines TNF-α and IL-6 was also suppressed in tumor cells in vitro and in tumor tissues in vivo ($P < 0.001$) (Figure 12e). Notably, GEVs also showed great potency in reducing the inflammation in tumors in comparison with the blank group, as reported in the literature. Thus, this evidence demonstrated the pronounced inflammation inhibitory competence of the nanodrug Tf-GEVs@Pt(IV) in tumors through inhibition of COX-2, TNF-α, and IL-6, which was ascribed to the synergistic functions of the ASP ligand and GEVs.

Reversing the Immune Inhibitory TME. The immunosuppressive environment, as another hallmark of cancer, poses a significant obstacle to cancer treatment. Fibrosis in tumors contributes to an immunosuppressive barrier to T cell infiltration, while the inflammatory TME is also a driving factor in immune suppression. The cGAS/STING pathway is a central component of the innate immune response signaling cascade, while platinum chemotherapy can induce the release of damaged dsDNA into the cytoplasm of cancer cells, further initiating the cGAS-STING pathway.[41,42] Herein, the immune modulating properties of Tf-GEVs@Pt(IV) in tumors were evaluated.

The RNA-seq analysis (Figures 7 and 13a,b) indicated that Tf-GEVs@Pt(IV) was potent in modulating genes relevant to immune responses, T cell activation, and macrophage activation. Moreover, the key checkpoint PD-L1/PD-1 and pathway cGAS/STING tightly associated with immunity, were highlighted.

Subsequently, immunohistochemical staining of T cells and macrophages in tumor tissues confirmed the significant competence of Tf-GEVs@Pt(IV) in promoting antitumor immunity (Figure 13e,f). The $CD3^+$ and $CD8^+$ T-cells increased by 22.7- and 20.8-fold higher to the blank group ($P < 0.001$). Meanwhile, the decrease of tumor-promoting $CD206^+$ M2 macrophages (15%, $P < 0.001$) and the increase of tumor-killing $CD86^+$ M1 macrophages (1911%, $P < 0.001$) compared to the blank group further validated the macrophage polarization from M2- to M1-type after Tf-GEVs@Pt(IV) treatment. Mechanism investigation by Western blotting and immunohistochemical staining assays was further conducted (Figure 13c–f). The immune checkpoint PD-L1 was significantly suppressed both in tumor cells in vitro ($P < 0.001$) and in tumor tissues in vivo ($P < 0.001$). Then, the cGAS/STING pathway was activated by the dsDNA released following the DNA damage caused by the platinum groups. The improved expression of STING, *p*-STING, TBK1, *p*-TBK1, IFR3, and *p*-IFR3 in 4T1 cells was also observed ($P < 0.001$), which indicated that the cGAS/STING pathway was involved during the treatment with Tf-GEVs@Pt(IV). Notably, the free complex **1** exerted a similar trend in modulating antitumor immunity both in vitro and in vivo, indicating that the immune-activating properties of Tf-GEVs@Pt(IV) were mainly ascribed to the active ingredient **1**.

Totally, the nanomedicine Tf-GEVs@Pt(IV) was promising in elevating antitumor immunity in tumors by causing T cell activation and macrophage shift from M2 to M1, which was mediated by activating the cGAS/STING pathway and blocking PD-L1 expression. The findings in this work were preliminary evidence for the immune modulating mechanism of Tf-GEVs@Pt(IV), and more work is highly deserved for further investigation in the future.

Mechanism of Action. The action mechanism of Tf-GEVs@Pt(IV) is proposed as Figure 14 based on the RNA-seq and experimental results above. The nanomedicine with GEVs as vehicles was effective in penetrating the fibrosis barrier to reach the tumor tissues. Then, the targeting motif Tf

https://doi.org/10.1021/acs.jmedchem.5c00815
J. Med. Chem. 2025, 68, 11928−11947

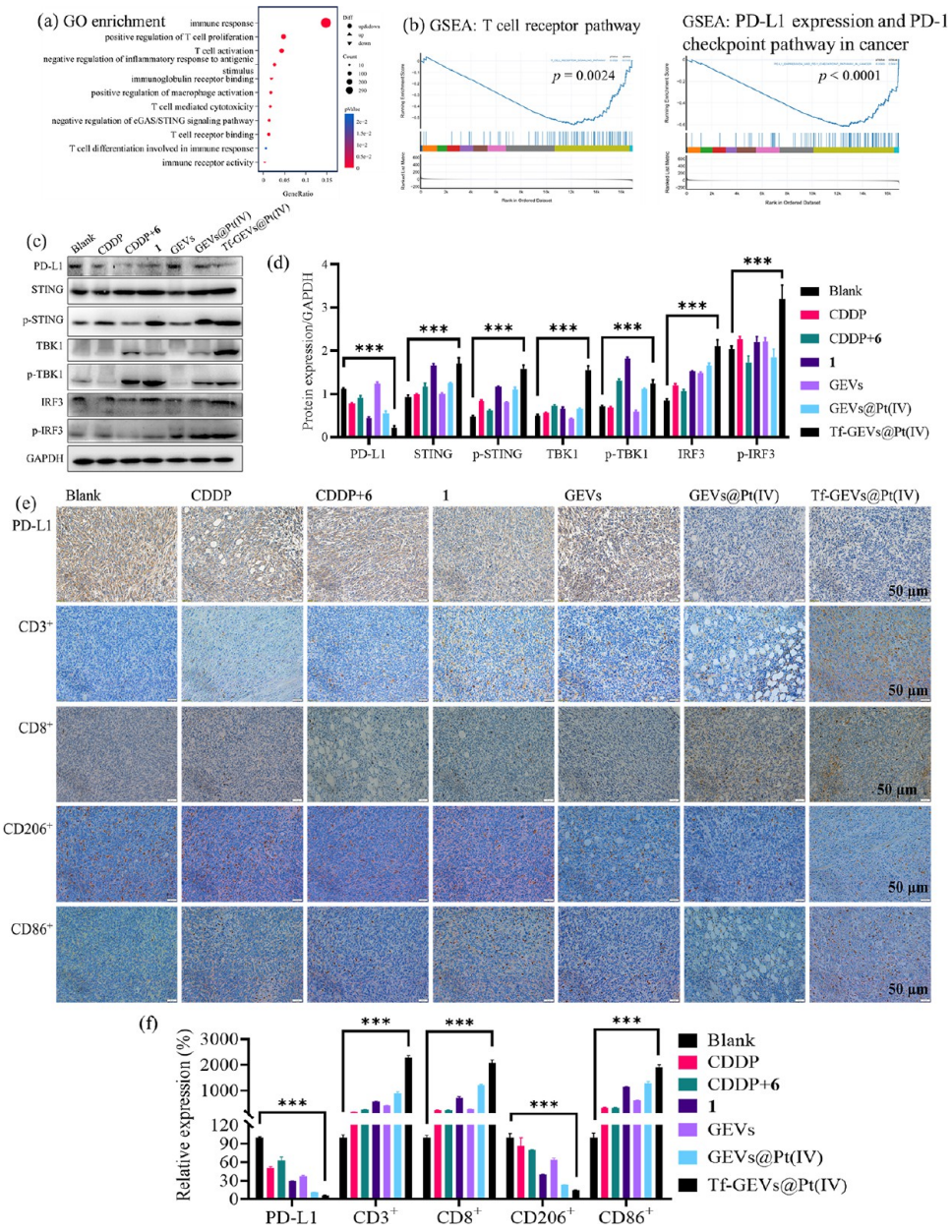

Figure 13. Properties in reversing immunosuppressive TME. (a, b) GO enrichment and GSEA analysis of the DEGs in blank vs Tf-GEVs@Pt(IV) concerning immunity. (c, d) Western blot analysis of PD-L1, STING, *p*-STING, TBK1, *p*-TBK1, IFR3, and *p*-IFR3 in 4T1 cells. (e, f) Immunohistochemical staining of PD-L1 expression, $CD3^+$ and $CD8^+$ T-cells, and $CD206^+$ M2- and $CD86^+$ M1-macrophages in tumor tissues from the antitumor experiments in vivo. ***$P < 0.001$.

significantly improved the tumor targeting properties, allowing the three-functional platinum(IV) active ingredient **1** to enter tumor cells at a higher level than the free complex, GEVs@Pt(IV), and the platinum(II) reference drugs. Then, conjugate **1** was reduced in the reducing TME to release the platinum(II), CTP, and ASP fragments. The platinum(II) complexes combined with DNA, causing significant DNA damage, and further improved the indicator proteins γ-H2AX and p53. Subsequently, mitochondria-mediated apoptosis was initiated through the Bcl-2/Bax/caspase-3 pathway by injuring the mitochondria and promoting ROS generation. The CTP endowed the nanodrug with the ability to inhibit fibrosis by suppressing the TGF-β1 and MMPs (MMP2, MMP9) cascades. As a result, collagen fibrosis was reduced in tumor tissues by decreasing the levels of α-SMA and FSP1. Consequently, the fibrosis barrier around the tumors was broken, which facilitated the penetration of drugs and immunocytes into the tumors. The inflammatory TME was significantly reversed after Tf-GEVs@Pt(IV) treatment, which was primarily attributed to the functions of GEVs and the ASP group. The key enzyme COX-2 was suppressed, and the secretion of inflammatory cytokines TNF-α and IL-6 was inhibited. Notably, the fibrotic and inflammatory TME promoted each other in tumors, and further synergistically recruited and stimulated the "cold" immunosuppressive TME into a 'hot' status. The PD-L1 as a pivotal immune checkpoint was blocked; meanwhile, the activation of the cGAS/STING pathway was also observed by monitoring the proteins STING, *p*-STING, TBK1, *p*-TBK1, IFR3, and *p*-IFR3. Consequently, the $CD3^+$ and $CD8^+$ T cells increased greatly, and macrophage

https://doi.org/10.1021/acs.jmedchem.5c00815
J. Med. Chem. 2025, 68, 11928−11947

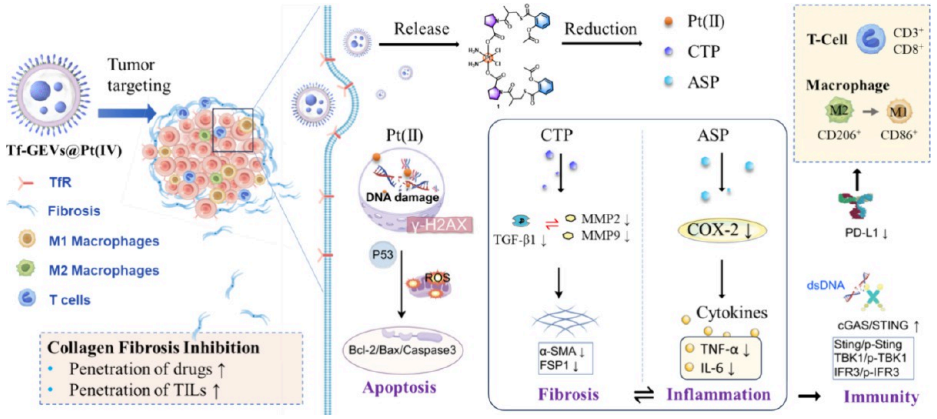

Figure 14. Proposed antitumor mechanism for Tf-GEVs@Pt(IV).

polarization from the M2- to M1-phenotype was induced. The multiple antitumor mechanisms of Tf-GEVs@Pt(IV) mentioned above are attributed to their promising antitumor activities, which offer a new strategy for the future design of novel and potent platinum(IV) antitumor agents.

CONCLUSIONS

The development of novel antitumor agents, especially potent ones with promising antimetastatic activities, represents a hot topic in the field of platinum drug investigation. Remodeling the TME during cancer treatment holds great promise in elevating the antitumor performance of drugs. Here, two three-functional platinum(IV) conjugates with an ingenious CTP-ASP ligand were designed and prepared. Hybrid **1** with dual ligands was identified as a candidate due to its potent antitumor activities against tumor cells in vitro ($IC_{50} \leq 4.18$ μM), which also showed great promise in reducing toxicity and overcoming the drug resistance of CDDP. The nanomedicine Tf-GEVs@Pt(IV) loading complex **1** was further prepared using GEVs as carriers. The in vivo tumor targeting and biodistribution study revealed that incorporating the tumor targeting motif Tf significantly improved the tumor targeting properties of Tf-GEVs@Pt(IV) compared to the nanodrug GEVs@Pt(IV) and the free complex **1**. Then, Tf-GEVs@Pt(IV) released the active ingredient **1** in tumors in a sustained manner, which allowed prolonged exposure of tumor cells to chemotherapeutics. As a result, Tf-GEVs@Pt(IV) displayed significant antigrowth activities in vivo with a higher TGI of 83.7% than GEVs@Pt(IV) (74.9%), and the free conjugate **1** (49.3%), as well as the references CDDP and CDDP+**6** (24.3%, 30.9%). More encouragingly, Tf-GEVs@Pt(IV) exhibited satisfactory activities against metastatic tumors both in vitro and in vivo. It inhibited the pulmonary metastasis models with an inhibitory rate of 88.1% in comparison with the blank group, higher than free complex **1** (72.6%), and the references CDDP (27.8%) and CDDP+**6** (51.3%). Notably, the antitumor immunity was provoked and displayed important roles in improving the antitumor activities. The bilateral homogenotypic 4T1 tumor models revealed that Tf-GEVs@Pt(IV) significantly suppressed the primary tumors with a high TGI = 79.4%, which further verified its promising antigrowth potency in vivo. More importantly, it led to a high TGI = 75.4% against the distant tumors, which was mainly attributed to the antitumor immunity in vivo; meanwhile, CDDP and CDDP+**6** showed rather lower activities (TGI = 16.5 and 27.1%, respectively). Then, the multispecific antitumor mechanism was extensively investigated. The three-functional platinum(IV) compound **1** was released from the nanomedicine Tf-GEVs@Pt(IV) in a sustained manner, which would be reduced to platinum(II), CTP, and ASP fragments. The platinum(II) core caused serious DNA damage and further promoted mitochondria-mediated apoptosis. The CTP ligand was potent in suppressing collagen fibrosis by inhibiting TGF-β1 and MMPs, and it further facilitated the penetration of drugs and immune cells into tumor tissues. Meanwhile, the ASP was pivotal in reducing the inflammatory TME by decreasing the COX-2 expression and cytokine levels. Moreover, the suppressed fibrotic and inflammatory TME reversed the immune-suppressive environment by inhibiting PD-L1 and activating cGAS/STING signaling, thereby promoting T-cell activation and a macrophage shift from M2 to M1. Notably, the influence of Tf-GEVs@Pt (IV) on TME was tightly involved in the antitumor activities based on the preliminary observations in this work, and further extensive investigations are highly warranted in future studies. These multiple antitumor mechanisms contributed to the promising antitumor performance of nanodrug Tf-GEVs@Pt(IV).

Summarily, the strengths of this work were highlighted as follows: (a) A series of novel three-functional platinum(IV) conjugates were developed by incorporating CTP-ASP ligands into the platinum(IV) system, which provided a new approach to constructing multifunctional platinum complexes. (b) The GEVs nanodrug loading platinum(IV) conjugates was developed and investigated, indicating the great potential of PDVs as vehicles of platinum(IV) complexes. (c) The tumor-targeting modification of the GEVs nanodrug improved the tumor-targeting capability, which further enhanced the antitumor activities both in vitro and in vivo. Accordingly, the nanodrug Tf-GEVs@Pt(IV) reported in this work deserves further investigation as an antitumor drug, especially against metastatic tumors, which may provide a new strategy for curing malignant cancers in clinical settings.

EXPERIMENTAL SECTION

General. The CDDP was sourced from Boyuan Pharmaceutical Co., Ltd. (Jinan, China). Other materials were obtained from Sigma, J&K, Aladdin, Macklin, and Innochem, and were used directly unless otherwise indicated. The reactions were carried out in a nitrogen environment with magnetic stirring. The ^{1}H NMR and ^{13}C NMR were recorded on a Bruker spectrometer operating at 500 and 126 MHz in deuterated solvents with TMS as the internal standard. The mass spectra (MS) were performed on a Shimadzu LC-MS/MS 8040

https://doi.org/10.1021/acs.jmedchem.5c00815
J. Med. Chem. 2025, 68, 11928−11947

mass spectrometer, while the high-resolution mass spectra (HRMS) were performed on a Waters G2-XS Q-TOF mass spectrometer. A Shimadzu AA-6880 instrument was used to perform atomic absorption spectroscopy (AAS) testing. The flow cytometry analysis was carried out with a Millipore Guava easyCyte 8HT flow cytometer. The HPLC spectra were recorded on a Thermo Ultimate 3000 RS or Shimadzu LC-20A spectrometer. All compounds were >95% pure, as determined by HPLC analysis.

Synthetic Procedure. *Preparation of Platinum(IV) Complex* ***1****.* Compound **6** (341 mg, 0.90 mmol) and TBTU (289 mg, 0.90 mmol) were dissolved in 5 mL of dry *N*,*N*-dimethylformamide (DMF) and stirred at room temperature for 15 min. Then, TEA (125 μL, 0.90 mmol) was added, and the mixture was stirred for an additional 15 min. After that, oxoplatin **7** (100 mg, 0.30 mmol) was added, and the mixture was stirred at 50 °C for 48 h in dark under nitrogen atmosphere. After the reaction was completed, the solvent was removed under vacuum and the crude product was purified by silica gel column chromatography to afford compound **1** as a yellow solid (101 mg, 32%). Its purity was 98.9% as determined by HPLC ($MeOH/H_2O$ = 70/30).

^1H NMR (500 MHz, DMSO-d_6) δ 7.95−7.60 (m, 3H), 7.55−7.41 (m, 2H), 7.28−7.10 (m, 1H), 7.03−6.86 (m, 2H), 6.45 (br, 6H, NH_3), 4.58−4.28 (m, 2H), 3.73−3.39 (m, 4H), 3.20−3.05 (m, 4H), 2.94−2.70 (m, 2H), 2.35−2.25 (m, 2H), 2.07−1.74 (m, 8H), 1.34−0.99 (m, 10H). ^{13}C NMR (126 MHz, DMSO-d_6) δ: 172.8, 167.7, 157.8, 137.7, 135.5, 134.6, 129.3, 122.7, 119.8, 118.1, 59.8, 46.0, 37.8, 32.1, 29.4, 24.4, 17.08, 9.1. MS-ESI: calcd for $[M + H]^+$: 1058 (M = $C_{36}H_{46}Cl_2N_4O_{12}PtS_2$), found: 1058. HRMS: calcd for $[M + NH_4]^+$: 1073.1917 (M = $C_{36}H_{46}Cl_2N_4O_{12}PtS_2$), found: 1073.1916.

Preparation of Platinum(IV) Complex ***2****.* Compound **6** (114 mg, 0.3 mmol) and TBTU (96 mg, 0.3 mmol) were dissolved in 5 mL of dry DMF and stirred at room temperature for 15 min. Then, TEA (42 μL, 0.3 mmol) was added, and the mixture was stirred for another 15 min. After that, oxoplatin **7** (100 mg, 0.3 mmol) was added. The mixture was stirred at 50 °C for 48 h in the dark under a nitrogen atmosphere. After the reaction was completed, the solvent was removed under a vacuum, and the crude product was purified by silica gel column chromatography to afford compound **2** as a yellow solid (58 mg, 28%). Its purity was 97.1%, as determined by HPLC ($MeOH/H_2O$ = 70/30).

^1H NMR (500 MHz, Methanol-d_4) δ 7.97−7.79 (m, 1H), 7.64−7.48 (m, 1H), 7.43−7.13 (m, 1H), 7.00−6.76 (m, 1H), 4.63−4.39 (m, 1H), 3.80−3.50 (m, 2H), 3.23−2.99 (m, 2H), 2.49−2.20 (m, 2H), 2.18−1.78 (m, 4H), 1.38−1.16 (m, 5H). ^{13}C NMR (126 MHz, Methanol-d_4) δ: 174.8, 174.1, 170.1, 166.3, 150.8, 133.5, 131.5, 125.7, 123.7, 123.5, 58.7, 42.2, 30.8, 28.9, 26.8, 24.3, 19.7, 15.7. MS-ESI: calcd for $[M + H]^+$: 695 (M = $C_{18}H_{27}Cl_2N_3O_7PtS$), found: 695. HRMS: calcd for $[M + Na]^+$: 717.0487 (M = $C_{18}H_{27}Cl_2N_3O_7PtS$), found: 717.0497.

Preparation of Platinum(IV) Complex ***3****.* Compound **8** (233 mg, 0.90 mmol) and TBTU (289 mg, 0.90 mmol) were dissolved in dry DMF (5 mL) and stirred at room temperature for 15 min. Then, TEA (125 μL, 0.90 mmol) was added, and the mixture was stirred for another 15 min. After that, oxoplatin **7** (100 mg, 0.30 mmol) was added. The mixture was stirred at 50 °C for 48 h in the dark under a nitrogen atmosphere. After the reaction was completed, the solvent was removed under vacuum, and the crude product was purified by silica gel column chromatography to afford compound **3** as a yellow solid (90 mg, 37%). Its purity was 98.5%, as determined by HPLC ($MeOH/H_2O$ = 70/30).

^1H NMR (500 MHz, DMSO-d_6) δ 4.56−4.15 (m, 2H), 3.66−3.40 (m, 4H), 3.04−2.71 (m, 6H), 2.59 (s, 3H), 2.43−2.30 (m, 3H), 2.23−2.07 (m, 2H), 1.96−1.83 (m, 4H), 1.28−1.20 (m, 2H), 1.14−0.98 (m, 6H). ^{13}C NMR (126 MHz, DMSO) δ: 195.9, 195.8, 173.3, 66.0, 58.8, 46.9, 37.8, 31.0, 29.5, 25.7, 16.9. MS-ESI: calcd for $[M]^+$: 816 (M = $C_{22}H_{38}Cl_2N_4O_8PtS_2$), found: 816. HRMS: calcd for $[M + Na]^+$: 838.1054 (M = $C_{22}H_{38}Cl_2N_4O_8PtS_2$), found: 838.1052.

Preparation of Platinum(IV) Complex ***4****.* Anhydride of ASP (307 mg, 0.9 mmol) and oxoplatin **7** (100 mg, 0.30 mmol) were dissolved in dry dimethyl sulfoxide (DMSO), 5 mL, and stirred at room temperature overnight. Then, the mixture was further stirred for 24 h at 65 °C. After the reaction was completed, the solvent was removed under a vacuum, and the crude product was purified by silica gel column chromatography to afford compound **4** as a pale yellow solid (69 mg, 35%). Its purity was 95.2% as determined by HPLC ($MeOH/H_2O$ = 85/15). Its purity was 99.4%, as determined by HPLC ($MeOH/H_2O$ = 70/30).

^1H NMR (500 MHz, DMSO-d_6) δ 7.93 (dd, J = 7.8, 1.7 Hz, 2H), 7.67−7.60 (m, 2H), 7.41−7.31 (m, 2H), 7.20 (dd, J = 8.1, 1.2 Hz, 2H), 5.86 (s, 2H), 2.25 (s, 6H). ^{13}C NMR (126 MHz, DMSO-d_6) δ: 169.7, 166.1, 150.6, 134.2, 131.8, 126.5, 124.6, 124.2, 21.3. MS-ESI: calcd for $[M + H]^+$: 659 (M = $C_{22}H_{38}Cl_2N_4O_8PtS_2$), found: 659.

Preparation of GEVs. The GEVs were prepared with the grapefruit as material using a differential centrifugation method with an ultracentrifuge (Beckman Optima XPN-100) based on the literature method (3000*g* for 30 min; 15,000*g* for 1 h; filtration through a 0.45 μm filter membrane; 100,000*g* for 2 h).[43,44] The concentration of GEVs was determined by the BCA protein quantification assay kit (Beyotime Biotechnology, China) and diluted to 2 mg/mL with PBS. Western blot analysis was employed to verify GEVs by measuring marker proteins Alix, CD9, and TSG101. The morphology was characterized by DLS and TEM.

Preparation of Nanoparticles DSPE-PEG@Pt(IV). The active ingredient **1** (20 mg) and DSPE-PEG_{2000} (20 mg) were dissolved in 0.4 mL of DMF (**1**:DSPE-PEG_{2000} = 1:1, w/w), and then the solution was dropped into 20 mL of PBS. The suspension was vigorously stirred for 15 min and homogenized by a D-3L homogenizer (PhD, USA) at an optimal homogenization condition of 100 MPa for 30 min. Then, the solution was dialyzed twice (MWCO 8−14 kDa) against PBS to remove the organic solvent, and the nanoparticles DSPE-PEG@Pt(IV) were obtained.

Preparation of Nanoparticles GEVs@Pt(IV) and Tf-GEVs@Pt(IV), and DiD-Labeled Nanoparticles DiD-GEVs@Pt(IV) and DiD-Tf-GEVs@Pt(IV). The GEVs were added to a solution of DSPE-PEG@Pt(IV) slowly (GEVs:**1** = 2:1, w/w). Subsequently, the solution was ultrasonicated for 3 min (300 W, 6 cycles of 30 s on/off, with 2 min intervals, $T \leq 10$ °C). Then, the solution was kept for 30 min at 37 °C to produce the GEVs-coated nanodrug GEVs@Pt(IV).[43] Subsequently, the Tf modified DSPE-PEG_{2000} (DSPE-PEG_{2000}-Tf) was added into the solution of GEVs@Pt(IV) (DSPE-PEG_{2000}-Tf/GEVs = 3:2, w/w). The mixture was incubated at 30 °C for 1 h,[45] and the Tf-GEVs@Pt(IV) was obtained. The morphology of the nanodrugs was characterized by DLS and TEM.

The DiD-labeled nanoparticles DiD-GEVs@Pt(IV) and DiD-Tf-GEVs@Pt(IV) were pared by dissolving DiD (1% of DSPE-PEG_{2000}, w/w) with complex **1** and DSPE-PEG_{2000} in DMF. The following procedures were the same as mentioned above.

Releasing Behavior of GEVs@Pt(IV) and Tf-GEVs@Pt(IV). The release behavior of GEVs@Pt(IV) and Tf-GEVs@Pt(IV) was analyzed in PBS media. The nanoparticles (5 mL) in dialysis bags (MWCO 8−14 kDa) were immersed in 100 mL of PBS, and the mixture was stirred at 37 °C (100 rpm). A solution of free complex **1** in 5 mL of PBS containing 5% DMF at the same concentration was prepared as an injection sample to compare with the nanodrugs. The release solution (3 mL) was withdrawn at predetermined time intervals, and fresh media (3 mL) were replenished. The concentration of drugs was determined using AAS by measuring the platinum content.

Cell Culture. The cells used in this study included four tumor cell lines: human lung cancer (A549), CDDP-resistant human lung cancer (A549R), murine breast cancer (4T1), and human liver cancer (HepG2), as well as one human normal liver cell line (LO2). These cell lines were maintained in our laboratory and procured from either the American Type Culture Collection (ATCC) or Pricella Biotechnology Company, Ltd. (Wuhan, China). Cells were cultured in DMEM (for HepG2) or RPMI 1640 (for A549, A549R, LO2, and 4T1 cells) supplemented with 10% fetal bovine serum (FBS) and 1% penicillin/streptomycin. All culture reagents were obtained from Sangon Biotec (China).

https://doi.org/10.1021/acs.jmedchem.5c00815
J. Med. Chem. 2025, 68, 11928−11947

Animals. All animals were purchased from Henan Skobes Biotechnology Co., Ltd. (Henan, China). The animals were housed under standard environmental conditions (12/12 h day/night cycle, 23 ± 2 °C) with free access to food and water. The experiments were conducted in full compliance with the NIH guidelines for the care and use of laboratory animals (NIH Publication 8023, revised 1978). The experiments were approved by the Institutional Animal Ethics Committee of Liaocheng University (No. AP2024022955). For the antitumor growth experiment in vivo, immune-competent female BALB/c mice (weighing 18−20 g, n = 35) were utilized. For antimetastatic experiments in vivo, female BALB/c mice (weighing 18−20 g, n = 35) were used. For activating the antitumor immunity experiment in vivo, female BALB/c mice (weighing 18−20 g, n = 35) were used. For tumor targeting studies in vivo, female BALB/c mice (weighing 18−20 g, n = 9) were used.

Antitumor Growth Assay in Vivo. The antitumor growth experiment was conducted on female BALB/c mice (18−20 g). Tumor-bearing models were established by injecting a suspension of tumor cells (1×10^6 in 0.15 mL of PBS) into the left flanks of the mice. The mice were divided into seven groups (blank, CDDP, CDDP+**6**, complex **1**, GEVs, GEVs@Pt(IV), and Tf-GEVs@Pt(IV), n = 5) on day 4. Mice were then injected with drugs intravenously (i.v.) through the tail vein at a dosage of 2 mg of Pt/kg on days 4, 7, and 10. The GEVs were administered in the same amount as that in the nanodrugs. Complex **1** and CDDP were dissolved in PBS with 5% DMF, and the blank group was injected with the free media. The volume of tumors was monitored daily ($V = W^2 \times L/2$, where W is the width and L is the length of the tumor), and the weight of the mice was also recorded. Mice were then sacrificed on day 12, and the tumor weight was measured. The TGI was calculated using the formula TGI = (1 − (tumor weight of the drug-treated group/tumor weight of the control group)) × 100%. The organs, including the heart, liver, spleen, lungs, kidneys, and tumors, were collected and fixed in 4% paraformaldehyde for 48 h. Subsequently, H&E staining and immunohistochemistry experiments were conducted.

Antitumor Assay against Metastatic Tumors In Vivo. The experiment was conducted on female BALB/c mice (18−20 g). Pulmonary metastasis models were established by injecting a suspension of tumor cells (1×10^5 in 0.2 mL of PBS) via a tail vein injection. The mice were divided into seven groups (blank, CDDP, CDDP+**6**, complex **1**, GEVs, GEVs@Pt(IV), and Tf-GEVs@Pt(IV), with n = 5). Mice were injected with drugs intravenously through the tail vein (i.v.) at a dosage of 2 mg Pt/kg on days 4, 7, and 10. The GEVs were administered in the same amount as the nanodrugs. Complex **1** and CDDP were dissolved in PBS with 5% DMF, and the blank group was injected with the free media. The GEVs were given in the same amount as those in the nanodrugs. Mice were sacrificed on day 12, and the lung tissues were collected. The nodules in each group were counted after being embedded in Bouin's fluid. The lungs were also stained using H&E staining to visualize the metastatic nodules within the lung tissues.

Antitumor Immunity Detection Assay In Vivo. To examine the antitumor immunity of the target agents in vivo, bilateral 4T1 tumor models on female immunocompetent BALB/c mice were employed in this study. The primary tumor was generated by injecting 1×10^6 cells into the left flank of the mice on day 0. The mice were then randomly divided into seven groups (blank, CDDP, CDDP+**6**, complex **1**, GEVs, GEVs@Pt(IV), and Tf-GEVs@Pt(IV), n = 5). Drugs were administered to the primary tumors via intratumoral injection (i.t.) on days 6, 9, and 12 at a dosage of 2 mg of Pt/kg. Complex **1** and CDDP were dissolved in PBS with 5% DMF, while the blank group was injected with free media. The GEVs were administered in the same amounts as those in the nanodrugs. On day 7, a distant tumor was generated by injecting 1×10^6 cells in the right flank of mice. The tumor volumes of both tumors were monitored during the experiment. The mice were sacrificed on day 15, and both tumor tissues were collected and measured. The TGI for both tumors was calculated.

Tumor Targeting Studies In Vivo. The tumor-targeting capabilities of the prepared nanodrugs were evaluated on female BALB/c mice (18−20 g) bearing murine 4T1 tumors using an IVIS optical imaging system (Alliance 4.7, UVITEC, Cambridge, UK) with the far-red fluorescence dye DiD as a probe. DiD was incorporated into nanomedicines to prepare DiD-GEVs@Pt(IV) and DiD-Tf-GEVs@Pt(IV). Tumor-bearing models were established by injecting 4T1 tumor cells (1×10^6 in 0.15 mL of PBS) subcutaneously into the left flanks of the mice. The experiment was conducted on day 7, when tumors had grown to 200−300 mm^3. Nine mice were randomly divided into three groups: DiD-**1**, DiD-GEVs@Pt(IV), and DiD-Tf-GEVs@Pt(IV). Drugs were injected (i.v.) at the same dosage of 2 mg of Pt/kg. Mice were briefly anesthetized with isoflurane inhalation and scanned using the IVIS system at 1, 2, 4, 8, 12, and 24 h. Afterward, the mice were sacrificed. The tissues, including the tumor, heart, liver, spleen, lung, and kidney, were collected and imaged by using the IVIS system. The tumor targeting and biodistribution results were analyzed based on the fluorescence intensity data.

■ ASSOCIATED CONTENT

Supporting Information

The Supporting Information is available free of charge at https://pubs.acs.org/doi/10.1021/acs.jmedchem.5c00815.

Synthesis of three-functional platinum(IV) complexes; stability of nanoparticles; release behavior of complex **1** from nanoparticles stability in biological media; uptake of drugs in tumor cells in vitro; antitumor activities in vivo; antimetastatic activities in vitro; RNA sequencing analysis; causing DNA damage; causing mitochondria-mediated apoptosis; experimental section; and ^{1}H NMR, ^{13}C NMR, MS, HRMS, and HPLC spectra (PDF)

Molecular formula strings (CSV)

■ AUTHOR INFORMATION

Corresponding Author

Qingpeng Wang − *Institute of Biopharmaceutical Research, State Key Laboratory of Macromolecular Drugs and Large-scale Preparation, Shandong Provincial Key Laboratory of Applied Technology for Protein and Peptide Drugs, Liaocheng University, Liaocheng 252059, P. R. China;* orcid.org/0000-0002-2093-8237; Email: lywqp@126.com

Authors

Yan Chen − *Institute of Biopharmaceutical Research, State Key Laboratory of Macromolecular Drugs and Large-scale Preparation, Shandong Provincial Key Laboratory of Applied Technology for Protein and Peptide Drugs, Liaocheng University, Liaocheng 252059, P. R. China*

Shuaiqi Feng − *Institute of Biopharmaceutical Research, State Key Laboratory of Macromolecular Drugs and Large-scale Preparation, Shandong Provincial Key Laboratory of Applied Technology for Protein and Peptide Drugs, Liaocheng University, Liaocheng 252059, P. R. China*

Lanjie Li − *Agricultural Science and Engineering School, Liaocheng University, Liaocheng 252059, P.R. China*

Guiqin Liu − *Agricultural Science and Engineering School, Liaocheng University, Liaocheng 252059, P.R. China*

Qingshan Ma − *Agricultural Science and Engineering School, Liaocheng University, Liaocheng 252059, P.R. China*

Zhifang Liu − *Institute of Biopharmaceutical Research, State Key Laboratory of Macromolecular Drugs and Large-scale Preparation, Shandong Provincial Key Laboratory of Applied Technology for Protein and Peptide Drugs, Liaocheng University, Liaocheng 252059, P. R. China*

Yanna Zhao − *Institute of Biopharmaceutical Research, State Key Laboratory of Macromolecular Drugs and Large-scale*

Preparation, Shandong Provincial Key Laboratory of Applied Technology for Protein and Peptide Drugs, Liaocheng University, Liaocheng 252059, P. R. China; orcid.org/0000-0001-9658-9996

Complete contact information is available at: https://pubs.acs.org/10.1021/acs.jmedchem.5c00815

Notes

The authors declare no competing financial interest.

■ ACKNOWLEDGMENTS

This work was supported by the Youth Innovation Technology Project of Higher School in Shandong Province (no. 2021KJ099), Natural Science Foundation of Shandong Province (no. ZR2020KH005), and National Natural Science Foundation of China (no. 21807056). This work was also technically supported by the State Key Laboratory of Macromolecular Drugs and Large-scale Preparation, Shandong Provincial Key Laboratory of Applied Technology for Protein and Peptide Drugs, Shandong Collaborative Innovation Center for Antibody Drugs, Engineering Research Center for Nanomedicine and Drug Delivery Systems, and Taishan Scholar Research Group. Some figures were drawn by FigDraw.

■ ABBREVIATIONS

AAS, atomic absorption spectrometry; ACE, angiotensin converting enzyme; AsA, ascorbic acid; CDDP, cisplatin; ASP, aspirin; COX-2, cyclooxygenase-2; CTP, captopril; DCFH-DA, 2′,7′-dichlorofluorescein diacetate; DLS, dynamic laser light scattering; DMF, *N,N*-dimethylformamide; DMSO, dimethyl sulfoxide; ECM, extracellular matrix; EVs, extracellular vesicles; GEVs, grapefruit-derived extracellular vesicles; 5′-GMP, guanosine-5′-monophosphate; H&E, hematoxylin-eosin; HPLC, high-performance liquid chromatography; IC_{50}, half maximal inhibitory concentration; IL, interleukin; i.v., intravenous injection; MMP, matrix metalloproteinase; MTT, (3-(4,5-Dimethylthiazol-2-yl)-2,5-diphenyltetrazolium bromide; NDDS, nanodrug delivery systems; PD-L1, programmed cell death-Ligand 1; PDVs, plant-derived extracellular vesicles; PI, propidium iodide; RF, resistant factor; RNA-seq, RNA-sequencing; ROS, reactive oxygen species; SI, selective index; TAI, tumor-associated inflammation; TBTU, *N,N,N′,N′*-tetramethyl-O-(benzotriazol-1-yl)uronium tetrafluoroborate; TEA, *N,N,N*-triethylamine; Tf, transferrin; TfR, transferrin receptor; TGI, tumor growth inhibition; TME, tumor microenvironment; TNF, tumor necrosis factor

■ REFERENCES

(1) Kiri, S.; Ryba, T. Cancer, metastasis, and the epigenome. *Mol. Cancer* **2024**, *23*, 154.
(2) Hill, W.; Weeden, C. E.; Swanton, C. Tumor promoters and opportunities for molecular cancer prevention. *Cancer Discovery* **2024**, *14*, 1154−1160.
(3) Xu, H.; Wen, J.; Yang, J.; Zhou, S.; Li, Y.; Xu, K.; Li, W.; Li, S. Tumor-microenvironment-on-a-chip: the construction and application. *Cell Commun. Signal.* **2024**, *22*, 515.
(4) Zhang, X.; Ma, H.; Gao, Y.; Liang, Y.; Du, Y.; Hao, S.; Ni, T. The tumor microenvironment: Signal transduction. *Biomolecules.* **2024**, *14*, 438.
(5) Piersma, B.; Hayward, M. K.; Weaver, V. M. Fibrosis and cancer: A strained relationship. *Biochim. Biophys. Acta Rev. Cancer.* **2020**, *1873*, No. 188356.
(6) Peng, D.; Fu, M.; Wang, M.; Wei, Y.; Wei, X. Targeting TGF-*β* signal transduction for fibrosis and cancer therapy. *Mol. Cancer* **2022**, *21*, 104.
(7) Acerbi, I.; Cassereau, L.; Dean, I.; Shi, Q.; Au, A.; Park, C.; Chen, Y. Y.; Liphardt, J.; Hwang, E. S.; Weaver, V. M. Human breast cancer invasion and aggression correlates with ECM stiffening and immune cell infiltration. *Integr. Biol.* **2015**, *7*, 1120−1134.
(8) Servais, C.; Erez, N. From sentinel cells to inflammatory culprits: cancer-associated fibroblasts in tumour-related inflammation. *J. Pathol.* **2013**, *229*, 198−207.
(9) Cohen, N.; Shani, O.; Raz, Y.; Sharon, Y.; Hoffman, D.; Abramovitz, L.; Erez, N. Fibroblasts drive an immunosuppressive and growth-promoting microenvironment in breast cancer via secretion of Chitinase 3-like 1. *Oncogene.* **2017**, *36*, 4457−4468.
(10) Zhu, Y.; Shi, C.; Zeng, L.; Liu, G.; Jiang, W.; Zhang, X.; Chen, S.; Guo, J.; Jian, X.; Ouyang, J.; Xia, J.; Kuang, C.; Fan, S.; Wu, X.; Wu, Y.; Zhou, W.; Guan, Y. High COX-2 expression in cancer-associated fibroblasts contributes to poor survival and promotes migration and invasiveness in nasopharyngeal carcinoma. *Mol. Carcinog.* **2020**, *59*, 265−280.
(11) Kennel, K. B.; Bozlar, M.; De Valk, A. F.; Greten, F. R. Cancer-associated fibroblasts in inflammation and antitumor immunity. *Clin. Cancer Res.* **2023**, *29*, 1009−1016.
(12) Coussens, L. M.; Werb, Z. Inflammation and cancer. *Nature.* **2002**, *420*, 860−867.
(13) Niland, S.; Riscanevo, A. X.; Eble, J. A. Matrix metalloproteinases shape the tumor microenvironment in cancer progression. *Int. J. Mol. Sci.* **2022**, *23*, 146.
(14) Tsoumakidou, M. The advent of immune stimulating CAFs in cancer. *Nat. Rev. Cancer.* **2023**, *23*, 258−269.
(15) Mao, X.; Xu, J.; Wang, W.; Liang, C.; Hua, J.; Liu, J.; Zhang, B.; Meng, Q.; Yu, X.; Shi, S. Crosstalk between cancer-associated fibroblasts and immune cells in the tumor microenvironment: new findings and future perspectives. *Mol. Cancer* **2021**, *20*, 131.
(16) Zhang, X.; Lao, M.; Yang, H.; Sun, K.; Dong, Y.; He, L.; Jiang, X.; Wu, H.; Jiang, Y.; Li, M.; Ying, H.; Liu, X.; Xu, J.; Chen, Y.; Zhang, H.; Zhou, R.; Gao, J.; Bai, X.; Liang, T. Targeting cancer-associated fibroblast autophagy renders pancreatic cancer eradicable with immunochemotherapy by inhibiting adaptive immune resistance. *Autophagy.* **2024**, *20*, 1314−1334.
(17) Barrett, R.; Puré, E. Cancer-associated fibroblasts: key determinants of tumor immunity and immunotherapy. *Curr. Opin. Immunol.* **2020**, *64*, 80−87.
(18) Zhang, C.; Xu, C.; Gao, X.; Yao, Q. Platinum-based drugs for cancer therapy and anti-tumor strategies. *Theranostics.* **2022**, *12*, 2115−2132.
(19) Yang, L.; Xie, H. J.; Li, Y. Y.; Wang, X.; Liu, X. X.; Mai, J. Molecular mechanisms of platinum-based chemotherapy resistance in ovarian cancer (Review). *Oncol. Rep.* **2022**, *47*, 82.
(20) Linares, J.; Sallent-Aragay, A.; Badia-Ramentol, J.; Recort-Bascuas, A.; Méndez, A.; Rupérez, N. M.; Re, D. L.; Rivas, E. I.; Guiu, M.; Zwick, M.; Iglesias, M.; Martinez-Ciarpaglini, C.; Tarazona, N.; Varese, M.; Hernando-Momblona, X.; Cañellas-Socias, A.; Orrillo, M.; Garrido, M.; Saoudi, N.; Elez, E.; Navarro, P.; Tabernero, J.; Gomis, R. R.; Batlle, E.; Pisonero, J.; Cervantes, A.; Montagut, C.; Calon, A. Long-term platinum-based drug accumulation in cancer-associated fibroblasts promotes colorectal cancer progression and resistance to therapy. *Nat. Commun.* **2023**, *14*, 746.
(21) Zhai, J.; Shen, J.; Xie, G.; Wu, J.; He, M.; Gao, L.; Zhang, Y.; Yao, X.; Shen, L. Cancer-associated fibroblasts-derived IL-8 mediates resistance to cisplatin in human gastric cancer. *Cancer Lett.* **2019**, *454*, 37−43.
(22) Puddephatt, R. J. Supramolecular organometallic chemistry: The platinum(IV) paradigm. *Dalton Trans.* **2022**, *51*, 7011−7024.
(23) Tan, X. X.; Li, G. S.; Wang, Q. P.; Wang, B. Q.; Li, D. C.; Wang, P. G. Small molecular platinum(IV) compounds as antitumor agents. *Prog. Chem.* **2018**, *30*, 831−846.

(24) Pathak, R. K.; Marrache, S.; Choi, J. H.; Berding, T. B.; Dhar, S. The prodrug platin-A: simultaneous release of cisplatin and aspirin. *Angew. Chem., Int. Ed. Engl.* **2014**, *53*, 1963−1967.
(25) Cheng, Q.; Shi, H.; Wang, H.; Min, Y.; Wang, J.; Liu, Y. The ligation of aspirin to cisplatin demonstrates significant synergistic effects on tumor cells. *Chem. Commun.* **2014**, *50*, 7427−7430.
(26) Brown, S.; Nores, G. D. G.; Sarker, A.; Ly, C.; Li, C.; Park, H. J.; Hespe, G. E.; Gardenier, J.; Kuonqui, K.; Campbell, A.; Shin, J.; Kataru, R. P.; Aras, O.; Mehrara, B. J. Topical captopril: a promising treatment for secondary lymphedema. *Transl. Res.* **2023**, *257*, 43−53.
(27) Shu, C.; Zheng, X.; Wang, Y.; Xu, Y.; Zhang, D.; Deng, S. Captopril inhibits matrix metalloproteinase activity and improves dentin bonding durability. *Clin. Oral. Investig.* **2022**, *26*, 3213−3225.
(28) Annana, S. K.; Ferdoush, J.; Lamia, F.; Roy, A.; Kar, P.; Nandi, M.; Kabir, M.; Saha, A. Computational insights into captopril's inhibitory potential against MMP9 and LCN2 in bladder cancer: Implications for therapeutic application. *Cancer Inform.* **2024**, *23*, No. 11769351241276759.
(29) Leng, G.; Duan, B.; Liu, J.; Li, S.; Zhao, W.; Wang, S.; Hou, G.; Qu, J. The advancements and prospective developments in anti-tumor targeted therapy. *Neoplasia.* **2024**, *56*, No. 101024.
(30) Zheng, S.; Li, G.; Shi, J.; Liu, X.; Li, M.; He, Z.; Tian, C.; Kamei, K. I. Emerging platinum(IV) prodrug nanotherapeutics: A new epoch for platinum-based cancer therapy. *J. Controlled Release* **2023**, *361*, 819−846.
(31) Lian, M. Q.; Chng, W. H.; Liang, J.; Yeo, H. Q.; Lee, C. K.; Belaid, M.; Tollemeto, M.; Wacker, M. G.; Czarny, B.; Pastorin, G. Plant-derived extracellular vesicles: Recent advancements and current challenges on their use for biomedical applications. *J. Extracell. Vesicles* **2022**, *11*, No. e12283.
(32) Elsharkasy, O. M.; Nordin, J. Z.; Hagey, D. W.; de Jong, O. G.; Schiffelers, R. M.; Andaloussi, S. E.; Vader, P. Extracellular vesicles as drug delivery systems: Why and how? *Adv. Drug Delivery Rev.* **2020**, *159*, 332−343.
(33) Herrmann, I. K.; Wood, M. J. A.; Fuhrmann, G. Extracellular vesicles as a next-generation drug delivery platform. *Nat. Nanotechnol.* **2021**, *16*, 748−759.
(34) Wiklander, O. P. B.; Mamand, D. R.; Mohammad, D. K.; Zheng, W.; Wiklander, R. J.; Sych, T.; Zickler, A. M.; Liang, X.; Sharma, H.; Lavado, A.; Bost, J.; Roudi, S.; Corso, G.; Lennaárd, A. J.; Valugerdi, M. A.; Mäger, I.; Alici, E.; Sezgin, E.; Nordin, J. Z.; Gupta, D.; Görgens, A.; El Andaloussi, S. Antibody-displaying extracellular vesicles for targeted cancer therapy. *Nat. Biomed. Eng.* **2024**, *8*, 1453−1468.
(35) Wang, B.; Zhuang, X.; Deng, Z. B.; Jiang, H.; Mu, J.; Wang, Q.; Xiang, X.; Guo, H.; Zhang, L.; Dryden, G.; Yan, J.; Miller, D.; Zhang, H. G. Targeted drug delivery to intestinal macrophages by bioactive nanovesicles released from grapefruit. *Mol. Ther.* **2014**, *22*, 522−534.
(36) Zhuang, X. Y.; Teng, Y.; Samykutty, A.; Mu, J.; Deng, Z.; Zhang, L.; Cao, P.; Rong, Y.; Yan, J.; Miller, D.; Zhang, H. G. Grapefruit-derived nanovectors delivering therapeutic miR17 through an intranasal route inhibit brain tumor progression. *Mol. Ther.* **2016**, *24*, 96−105.
(37) Niu, W.; Xiao, Q.; Wang, X.; Zhu, J.; Li, J.; Liang, X.; Peng, Y.; Wu, C.; Lu, R.; Pan, Y.; Luo, J.; Zhong, X.; He, H.; Rong, Z.; Fan, J. B.; Wang, Y. A biomimetic drug delivery system by integrating grapefruit extracellular vesicles and doxorubicin-loaded heparin-based nanoparticles for glioma therapy. *Nano Lett.* **2021**, *21*, 1484−1492.
(38) Mojarad-Jabali, S.; Mahdinloo, S.; Farshbaf, M.; Sarfraz, M.; Fatahi, Y.; Atyabi, F.; Valizadeh, H. Transferrin receptor-mediated liposomal drug delivery: Recent trends in targeted therapy of cancer. *Expert Opin. Drug Del.* **2022**, *19*, 685−705.
(39) Zhang, M.; Chen, Y.; Feng, S.; He, Y.; Liu, Z.; Zhang, N.; Wang, Q. Transferrin-modified carprofen platinum(IV) nanoparticles as antimetastasis agents with tumor targeting, inflammation inhibition, epithelial-mesenchymal transition suppression, and immune activation properties. *J. Med. Chem.* **2024**, *67*, 16416−16434.
(40) Guan, Q.; Li, Y.; Zhang, H.; Liu, S.; Ding, Z.; Fan, Z.; Wang, Q.; Wang, Z.; Han, J.; Liu, M.; Zhao, Y. Laser-responsive multifunctional nanoparticles for efficient combinational chemo-photodynamic therapy against breast cancer. *Colloids Surf. B Biointerfaces.* **2022**, *216*, No. 112574.
(41) Liu, J.; Liu, C.; Ma, Y.; Pan, X.; Chu, R.; Yao, S.; Chen, J.; Liu, C.; Chen, Z.; Sheng, C.; Zhang, K.; Xue, Y.; Schiöth, H. B.; Kong, B.; Zhang, Q.; Song, K. STING inhibitors sensitize platinum chemotherapy in ovarian cancer by inhibiting the cGAS-STING pathway in cancer-associated fibroblasts (CAFs). *Cancer Lett.* **2024**, *588*, No. 216700.
(42) Hu, J.; Sánchez-Rivera, F. J.; Wang, Z.; Johnson, G. N.; Ho, Y. J.; Ganesh, K.; Umeda, S.; Gan, S.; Mujal, A.; Delconte, R. B.; Hampton, J. P.; Zhao, H.; Kottapalli, S.; de Stanchina, E.; Iacobuzio-Donahue, C. A.; Pe'er, D.; Lowe, S. W.; Sun, J. C.; Massagué, J. STING inhibits the reactivation of dormant metastasis in lung adenocarcinoma. *Nature.* **2023**, *616*, 806−813.
(43) Li, M.; Tai, Q.; Shen, S.; Gao, M.; Zhang, X. Biomimetic exosome-sheathed magnetic mesoporous anchor with modification of glucose oxidase for synergistic targeting and starving tumor cells. *ACS Appl. Mater. Interfaces.* **2024**, *16* (23), 29634−29644.
(44) Man, F.; Meng, C.; Liu, Y.; Wang, Y.; Zhou, Y.; Ma, J.; Lu, R. The study of ginger-derived extracellular vesicles as a natural nanoscale drug carrier and their intestinal absorption in rats. *AAPS PharmSciTech* **2021**, *22* (6), 206.
(45) Li, D.; Yao, S.; Zhou, Z.; Shi, J.; Huang, Z.; Wu, Z. Hyaluronan decoration of milk exosomes directs tumor-specific delivery of doxorubicin. *Carbohydr. Res.* **2020**, *493*, No. 108032.

https://doi.org/10.1021/acs.jmedchem.5c00815
J. Med. Chem. 2025, 68, 11928−11947